08

STIF

Supplement to III

E7.5 10.1.94
CR-142343

AUTOMATED THEMATIC MAPPING AND CHANGE DETECTION OF ERTS-A IMAGES

Nicholas Gramenopoulos
Optical Systems Division
Itek Corporation
10 Maguire Road
Lexington, Massachusetts 02173

February 1975
Final Report

Prepared for
GODDARD SPACE FLIGHT CENTER
Greenbelt, Maryland 20771

1074A

AUTOMATED THEMATIC MAPPING AND CHANGE DETECTION OF ERTS-A IMAGES

Nicholas Gramenopoulos
Optical Systems Division
Itek Corporation
10 Maguire Road
Lexington, Massachusetts 02173

February 1975
Final Report

Prepared for
GODDARD SPACE FLIGHT CENTER
Greenbelt, Maryland 20771

TECHNICAL REPORT STANDARD TITLE PAGE

1. Report No.	2. Government Accession No.	3. Recipient's Catalog No.

4. Title and Subtitle	5. Report Date
Automated Thematic Mapping and Change Detection of ERTS-A Images	February 1975
	6. Performing Organization Code
7. Author(s) Nicholas Gramenopoulos PR 504	8. Performing Organization Report No.
9. Performing Organization Name and Address Optical Systems Division Itek Corporation 10 Maguire Road Lexington, Massachusetts 02173	10. Work Unit No.
	11. Contract or Grant No. NAS5-21766
12. Sponsoring Agency Name and Address	13. Type of Report and Period Covered
	14. Sponsoring Agency Code

15. Supplementary Notes

16. Abstract

In the first part of the investigation, spatial and spectral features were developed which were employed to automatically recognize terrain features through a clustering algorithm.

In this part of the investigation, the size of the cell which is the number of digital picture elements used for computing the spatial and spectral features was varied. It was determined that the accuracy of terrain recognition decreases slowly as the cell size is reduced and coincides with increased cluster diffuseness.

It was also proven that a cell size of 17 x 17 pixels when used with the clustering algorithm results in high recognition rates for major terrain classes. This cell size also permits the clustering of terrain subclasses. ERTS-1 data from five diverse geographic regions of the United States was processed through the clustering algorithm with 17 x 17 pixels cells. Simple land use maps were produced and the average terrain recognition accuracy was 82%.

17. Key Words (Selected by Author(s))	18. Distribution Statement
Interpretation Techniques Development, Digital Information Extraction Techniques, Classification and Pattern Recognition.	

19. Security Classif. (of this report)	20. Security Classif. (of this page)	21. No. of Pages	22. Price*
Unclassified	Unclassified	67	

*For sale by the Clearinghouse for Federal Scientific and Technical Information, Springfield, Virginia 22151.

PREFACE

A. OBJECTIVE

The main objective of this part of the investigation is to expand and refine the digital interpretation techniques developed during the first part of the investigation completed in July 1974 (see Reference 1).

The computer recognition of terrain is based on the classification of seven-dimensional vectors, computed from ERTS-1 data cells. Each cell contains 32 x 32 picture elements and represents an area 2.5 kilometers square on the surface of the earth. It is desirable to reduce the cell size in order to achieve better definition of boundaries between terrain types.

The main thrusts of the present investigation are: to determine the effects of cell size on the terrain recognition accuracy and to explore the characteristics of the clustering algorithm by processing digital ERTS data from additional geographic regions with substantially different terrain features.

B. SCOPE OF WORK

The work performed in this part of the investigation was divided into three major tasks:

1. The software was modified to permit the interpretation of ERTS-1 data with any cell size. Then, ERTS-1 data was processed at several cell sizes and the behavior of vector statistics as the cell size is reduced was analyzed. Finally, the accuracy of terrain recognition as affected by cell size was determined.

2. The interpretation results from several cell sizes were analyzed in order to examine the possibility of second level classification by which additional terrain classes or subclasses are recognized by combining the interpretation results from several cell sizes.

3. In the final task, it was established that 17 x 17 pixels cells could be used with the clustering algorithm to recognize terrain classes with high accuracy. Greater experience with this size cell and the clustering algorithm was gained by processing data from five ERTS-1 images representing diverse geographic regions of the United States.

This report describes the work performed and the results obtained.

C. CONCLUSIONS

The results of this part of the investigation showed that the accuracy of terrain recognition decreases slowly with the cell size. In addition, for the smallest cell sizes investigated (9 x 9 pixels and 13 x 13 pixels), the number of terrain classes that are recognized decreases. The reduction in the terrain detection rates coincides with increased cluster diffuseness as the cell size is reduced. The cluster diffuseness was ascertained by decreased divergence values between the clusters and increased cluster variances.

This investigation has proven that a cell size of 17 x 17 pixels when used with the clustering algorithm often results in a larger number of classes being recognized than when the 32 x 32 pixels cell is employed. For a given area, the 17 x 17 pixels cell produces 3.5 times more vectors than the 32 x 32 pixels cell, thus allowing the formation of clusters which represent terrain classes of small area size. For example, if the 32 x 32 pixels cell is used, an urban cluster representing a small city will not be formed due to an insufficient number of vectors from the urban cells, and perhaps only one urban cluster of a metropolitan area will be formed. If the 17 x 17 pixels cell is used, there are 3.5 times more urban vectors, so a cluster representing a small city could be formed while a metropolitan area may produce 2-4 urban clusters. Hence, second-level classification by which subclasses of the major terrain classes are formed, is possible with the 17 x 17 pixels cell. The average detection rate with the 17 x 17 pixels cell is about 82%, while the average detection rate with the 32 x 32 pixels cell is about 89%. It appears that the 17 x 17 pixels cell is a good nominal cell size and depending on the specific geographic region and the terrain accuracy requirements, this nominal cell size may be varied.

D. RECOMMENDATIONS

The interpretation techniques and software developed during this investigation have been thoroughly analyzed and tested by processing ERTS-1 data from diverse geographic regions of the United States. It is our opinion that land use maps can be produced by computer processing using these techniques and software on a competitive basis with human photointerpretation. Furthermore, machine interpretation is the only practical means of utilizing the huge volume of data produced by the earth resources satellites. The trends in microcircuit technology point to more

powerful and cheaper computers in the future. In addition, earth resources satellites with better ground resolutions and higher data capacities are being planned for the future. Therefore, it is recommended that greater efforts should be made to apply the ERTS-1 data and machine interpretation on real problems of national importance. The following applications are suggested as being potentially of high economic value:

a. Monitoring of agricultural crops and forest resources to detect crop stresses and estimate crop yield.

b. Uniform land use mapping of the entire country.

c. Monitoring of snow fields to predict flooding and estimate water resources.

d. Detection of water pollution.

The interpretation techniques and software developed under this investigation should now be applied on specific earth resources monitoring and management problems. Furthermore, hardware implementations of these techniques should be developed in order to further improve the speed and cost-effectiveness of machine interpretation of earth resources data.

TABLE OF CONTENTS

LIST OF FIGURES

LIST OF FIGURES
(Continued)

LIST OF TABLES

LIST OF TABLES
(Continued)

1. INTRODUCTION

This is the final report for this investigation and covers the technical work done and the results achieved over the period of June 1974 through January 1975 under an extension of the NASA Contract NAS5-21766. The work performed during this period is a continuation of the development of automatic interpretation techniques that was performed under Contract NAS5-21766. Therefore, the previous reports of this investigation appearing in the references and particularly the final report (Reference 1) of July 1974, provide a very useful background for the work described in the following sections.

The main body of the report is divided into the following sections:

A. Input Data Operations, which describes the digital preprocessing operations on the ERTS Digital Tapes (Bulk CCT's) necessary for the preparation of the digital data for the subsequent feature computation and clustering operations.

B. Terrain Recognition versus Cell Size. This section describes the experiments that were performed to determine the dependence of the terrain recognition on the cell size employed.

C. Second Level Classification Results. This section describes the results achieved when the terrain classifications with different cell sizes over a given area are combined in order to increase the number of terrain classes that can be recognized.

D. Applications of Clustering Algorithm. The clustering algorithm has been applied to digital data from five geographic regions of the United States with different terrain characteristics. The classification results obtained are described in this section.

E. Conclusions.

F. Recommendations.

2. INPUT DATA OPERATIONS

A number of digital operations are required to utilize the data available in the system corrected Computer Compatible Tapes (CCT's) that were provided by NDPF. Each computer compatible tape contains one-quarter of an ERTS image. The four spectral bands (for an MSS image) are interleaved. In addition, the sampling interval (in meters) along a scan line is smaller than the sampling interval between scan lines. In other words, there are more picture elements along a kilometer on the surface of the earth parallel to a scan line (approximately east-west direction) than a kilometer normal to a scan line (approximately north-south direction). Furthermore, successive lines are slightly shifted to each other, owing to the earth's rotation in relation to the satellite velocity.

The first preprocessing operation requires the separation of the MSS 4, 5, and 7 spectral bands into separate digital images consisting of 810 samples per scan line and 1,000 scan lines each. The 1,000 scan lines are selected from each CCT (which contains 2,340 lines) so that they cover approximately the north-south extent of a test site. To cover the east-west extent of a test site, it is necessary to combine data from two adjacent CCT's. So, the first preprocessing operation involves stripping data from two CCT's and producing six images (two in each spectral band), containing 810 x 1,000 samples each.

The second preprocessing operation combines adjacent images, so one is left with three images (one in each spectral band) containing 1,620 x 1,000 samples each. These images have a major distortion which is an enlargement of the images in the scanning direction (east-west approximately) and results from the unequal sample spacing in the scanning and raster directions. Visually, the images look like oblique rather than vertical photographs. This image distortion causes artificial variations in the spatial signatures of the terrain types. For example, a square farm would appear as a rectangle or a skewed parallelogram depending on its orientation to the scanning direction. It is necessary, therefore, to resample each image in the scanning direction in order to equalize the sample spacing in the two orthogonal directions.

A minor geometric distortion is a slight skewness, typically 3-3.5 degrees due to the earth's rotation.

The third preprocessing operation involves resampling of the images in the scanning direction and reducing the samples from 1,620 samples per line to 1,170 samples per line. During the first part of the investigation completed before

June 1974, the resampling operation was performed by taking the Fourier transform of each scan line, and then taking the inverse Fourier transform using only the first 1,170 Fourier transform samples. The resulting interpolation was very accurate except for some ringing effects at the beginning and end of the scan line. In addition, no correction was then applied for the geometric skewness mentioned above. In the second part of the investigation, it was expected that the spatial features of the various terrain categories would become less distinct as the cell size was reduced. Therefore, it was desirable to eliminate any known sources of noise in the spatial features, such as the skewness in the data.

The old sample interpolation technique using the Fourier transforms would have to be modified in order to correct for the skewness. Furthermore, it was a computationally very slow operation. It was, therefore, decided to replace it with a new quadratic interpolation technique which is considerably faster and can easily accommodate the skewness correction. This interpolation technique works as follows:

a. The input sample spacing is T_1 and the output sample spacing is T_2, where

$$T_2 = \frac{1,620}{1,170} T_1 \qquad (2\text{-}1)$$

b. The skewness correction amounts to a shift Δj to the right for the jth scan line. The resampled output image appears schematically in Figure 2-1. The first scan line has the largest shift and the last scan line has a minimum shift. As seen in Figure 2-1, the output image has two wedges on its left and right sides filled with zeros. The maximum shift is typically about 60 pixels. In fact,

$$\Delta_1 = N\alpha \qquad (2\text{-}2)$$

where N = number of scan lines
α = skew angle in radians.
Typically, $N = 1,000$ and $\alpha = 0.050 - 0.065$.

The shifting does not vary continuously between successive scan lines, but changes abruptly between groups of six scan lines. In other words, six successive scan lines have the same shift, then the next group of six scan lines has a slightly different shift, etc.

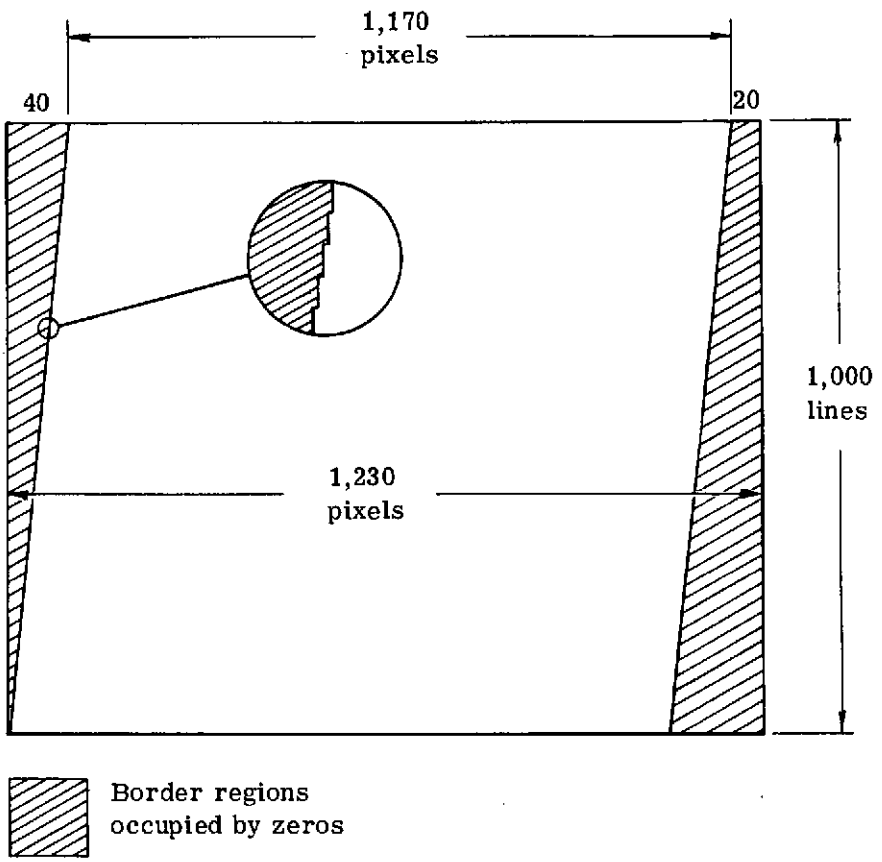

Fig. 2-1 — Resampled image geometry

c. A transformation relates the input and output images. Using this transformation, the location of an output image pixel in relation to the input image pixels can be determined. The transformation is

$$X_{ij} = iT_2 - \Delta j \qquad (2\text{-}3)$$

where X_{ij} = location of the ith output pixel in the jth scan line.

If X_{ij} is negative, a zero is inserted as the ith pixel in the jth line of the output image. If X_{ij} is positive, the nearest (kth) input image pixel is determined so that

$$|X_{ij} - kT_1| \leq \left(\frac{T_1}{2}\right) \qquad (2\text{-}4)$$

If k = 1, then the 1st, 2nd and 3rd input pixels are used in the interpolation. If k = 1,620, then the 1,618th, 1,619th and 1,620th pixels are used in the interpolation. Otherwise, the (k-1)th, kth and (k+1)th pixels are used in the interpolation.

d. In the vicinity of the kth pixel, the input image is approximated by a quadratic function f(x) such that

$$f(x) = a + bx + cx^2 \qquad (2\text{-}5)$$

Let $x_1 = (k-1)T_1$
$x_2 = (k)T_1$
$x_3 = (k+1)T_1$

and f_1 = amplitude of (k-1)th pixel
f_2 = amplitude of kth pixel
f_3 = amplitude of (k+1)th pixel.

Then, the following equations are formed:

$$\begin{aligned} f_1 &= a + bx_1 + cx_1^2 \\ f_2 &= a + bx_2 + cx_2^2 \\ f_3 &= a + bx_3 + cx_3^2 \end{aligned} \qquad (2\text{-}6)$$

The parameters a, b and c are determined by solving these equations. Finally, the amplitude of the output pixel (f_{ij}) is computed from the following equation

$$f_{ij} = a + bx_{ij} + cx_{ij}^2 \qquad (2\text{-}7)$$

After this resampling operation, the scale of the images is approximately the same in all directions.

The fourth preprocessing operation records the digital images as transparencies in a recorder for visual examination. This is necessary since some images display missing lines and a few images have pronounced line structure. The line structure with periodicity of six lines seems to arise from inaccurate calibration of the MSS detectors (there are six detectors per spectral band).

The MSS images produced by ERTS-1 in 1973 and 1974 had less noise and it was not necessary to employ two additional preprocessing operations that had been devised in the first part of the investigation to filter out the detector noise.

The preprocessing operations have been completed for the following ERTS-1 images:

1031 - 17325 from Phoenix, Arizona
1080 - 15192 from Washington D. C.
1258 - 15082 from New York, New York
1090 - 18012 from Los Angeles, California
1273 - 18183 from San Francisco, California
1376 - 17452 from Hill County, Montana.

3. TERRAIN RECOGNITION VERSUS CELL SIZE

3.1 Computation of Spatial Features

The cell size that was employed in the first part of the investigation was 32 x 32 picture elements which corresponds to about 2.5 x 2.5 kilometers on the surface of the earth. In order to compute the spatial features of a cell, the Fourier transform of the cell must be first computed digitally. The Fourier transform is a matrix of 32 x 32 complex numbers, which represent spatial frequencies ranging from 0.39 to 5.9 cycles per kilometer. Because the image pixels are real numbers, the Fourier transform samples located symmetrically opposite each other in relation to the Fourier transform origin have the property that their amplitudes are equal and their phases are equal and of opposite polarity. If the cell size is reduced to 16 x 16 pixels, then the Fourier transform is also reduced in size to 16 x 16 samples representing a frequency range of 0.78 to 5.9 cycles per kilometer. The maximum frequency in the transform (5.9 cycles per kilometer) is the same regardless of the cell size and is related only to the ground sampling interval of the ERTS Multi-Spectral Scanner (MSS). On the other hand, the frequency resolution of the Fourier transform which is equal to the frequency increment between successive transform samples is inversely proportional to the cell size. To illustrate how a sinusoidal frequency component of ground reflectance appears in the Fourier transform, consider the following example:

a. Assume that the ground reflectance is constant except for an one-dimensional sinusoidal variation of frequency f_o cycles per kilometer. Assume, further, that the cell size is PxP kilometers.

b. The continuous Fourier transform is shown in Figure 3-1. The Fourier transform is a two-dimensional sinc function centered at $f = f_o$. In fact, this function is

$$F(f_x, f_y) = \frac{\sin \pi (f_x - f_o)P}{\pi (f_x - f_o)P} \cdot \frac{\sin \pi f_y P}{\pi f_y P} \qquad (3\text{-}1)$$

The first zeros of this function occur at frequency increments Δf from the frequency peak at $f = f_o$,

$$\text{where, } \Delta f = 1/P \qquad (3\text{-}2)$$

Figure 3-1 also shows the Fourier transform samples of the digital Fourier transform which are spaced at multiples of (1/P) cycles per kilometer. If f_o is a multiple of (1/P), then one sample will be located at $f = f_o$ and will sample the maximum value of the sinc function of Eq. (3-1). In addition, all other samples will be

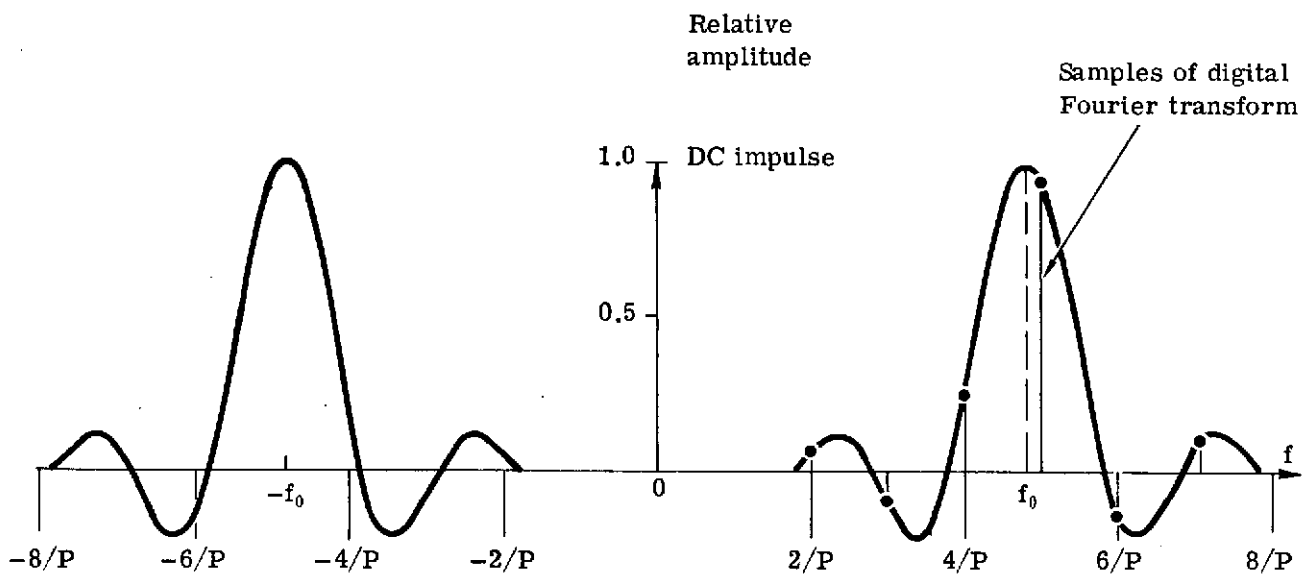

Fig. 3-1 — Fourier transform of sinusoidal brightness distribution

zero because they will coincide with the zeros of the sinc function. If f_o is not a multiple of (1/P), then there will be two large samples at $(f_o - 1/P) < f < (f_o + 1/P)$ and other samples will be small, but not zero. This shows that a frequency f_o present in the image does not appear as a single sample in the Fourier transform. Furthermore, as the cell size is reduced, P becomes smaller, the sample interval (1/P) becomes larger and the sinc function becomes wider. It is clear, then, that the Fourier transform cannot resolve frequencies separated by less than (1/P) cycles per kilometer and as the cell size is reduced, the frequency resolution of the Fourier transform becomes coarser.

The spatial features are computed from the digital Fourier transform. Certain regions of the transform are excluded (see Figure 3-2) for the following reasons.

a. The vertical column through the origin is excluded because it was found to contain substantial detector calibration noise even though the corresponding image may not show an obvious scan line structure.

b. The corners of the Fourier transform which lie beyond a radius of 5.9 cycles per kilometer from the origin of the transform are excluded so that the transform will have circular symmetry. The intent is to make the spatial features independent of the relative azimuth orientation of the terrain to the scanning direction of the multispectral scanner (MSS).

c. It was determined in the first part of the investigation that spatial frequencies less than 3.5 cycles/km were not contributing to terrain recognition and that better results could be achieved by excluding these frequencies. For this reason, a circular core of the transform with a radius of 3.5 cycles/km is excluded.

The remaining portions of the Fourier transform which are used to compute the spatial features consist of the two half doughnuts shown in Figure 3-2. Then, measurements of four spatial features are made as follows:

a. The largest peak (or maximum) is determined.

b. The energy in a sector which is $\pi/8$ radians wide and centered on the largest peak is determined. The energy is defined as the sum of the amplitudes of the Fourier transform samples within the sector and constitutes the first spatial feature S_1.

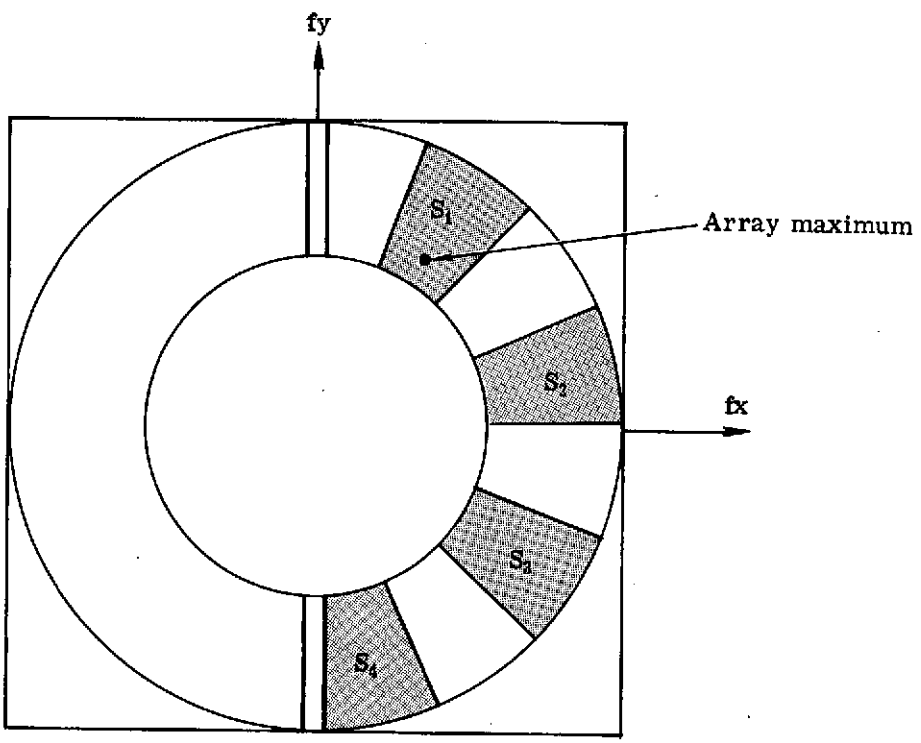

Fig. 3-2 — Fourier transform integration regions

c. The energies in similar size sectors which are displaced from the first one by $\pi/4$, $\pi/2$ and $3\pi/4$ radians in a clockwise direction are also determined and constitute the features S_2, S_3 and S_4, respectively. (See Figure 3-2)

The features S_1, S_2, S_3 and S_4 are each the sumon the average of 33 samples when the cell size is 32 x 32 pixels and about 7 samples when the cell size is 16 x 16 pixels. The decision whether a sample is within the sector of S_1 is made by an algorithm which compares the sample's location in relation to the angular boundaries of the sector. The location of the sector boundaries depend on the location of the maximum transform sample which lies along the centerline of the S_1 sector. Therefore, the boundaries of the sectors are variable between different image cells and the number of samples summed to produce S_1, S_2, S_3 and S_4 is not constant. This causes a random quantization error in the spatial features which is more serious for the small cell size where on the average a small number of samples are summed to produce the spatial features.

3.2 Fourier Transform Interpolation

It was decided to increase the number of samples available in the Fourier transform regardless of the cell size in order to reduce the quantization noise. Since the number of independent transform samples is the same as the number of cell pixels, the number of transform samples can be increased by interpolation. The interpolation is fairly simple if the new samples are to be located half way between the old samples. In this case, it is preferable if the cell size is an odd number such as 33 x 33 or 17 x 17. Introducing new samples between the old ones, a 17 x 17 samples transform can be interpolated to a 33 x 33 samples transform. It should be noted that the interpolated 33 x 33 samples transform does not have the frequency resolution of a transform computed from a 33 x 33 pixels cell.

The frequency resolution of an interpolated Fourier transform is (1/P) where P is the cell size from which the transform was computed. The interpolation reduces the quantization error associated with the boundaries of the sectors. It was decided to interpolate the Fourier transform as many times as is necessary so that the spatial features would not be computed on transforms smaller than 33 x 33 samples. This is accomplished as follows:

a. A transform larger than 17 x 17 samples is interpolated once so that the interpolated transform will be larger than 33 x 33 samples.

b. A transform larger than 9 x 9, but smaller than 17 x 17 samples is interpolated twice.

c. A transform larger than 5 x 5, but smaller than 9 x 9 samples is interpolated three times.

The interpolation technique employed is linear. A new sample is the average of the two adjacent old samples. First, the interpolation along the transform's rows is completed. Then, new rows are interpolated by averaging adjacent rows. For example, a new second row is created by averaging the original first and second rows. Then, the original second row becomes the third row, etc. Figure 3-3 demonstrates the interpolation technique.

In order to be able to select the desirable cell size, the software was modified to permit computations of the spatial features from any odd size cell. In addition, the interpolation routine was added so that the interpolated transform would have at least 33 x 33 samples.

3.3 Variations in the Features versus Cell Size

3.3.1 Amplitude Transformations of Features

As the cell size is decreased, it is expected that random errors and variations in the features increase while systematic differences due to the terrain classes are reduced. The effects of cell size on the spatial features and the terrain recognition accuracy were investigated on ERTS-1 image 1031-17325 from Phoenix, Arizona. This image had been used in the first part of the investigation and interpretation results for cells containing 32 x 32 pixels were available.

During the second part of the investigation, image 1031-17325 was processed through the clustering algorithm at three different cell sizes: 17 x 17 pixels, 13 x 13 pixels, and 9 x 9 pixels. The smallest pixel size gave the poorest results. In addition, it was observed that the interpretation results (see Section 3.4) became progressively worse as the cell size was reduced.

Each cell is represented by a seven-dimensional feature vector. The first component of the vector is a derivative count. In other words, the derivative of each cell in the MSS 5 band is taken and the number of pixels exceeding a set threshold are counted. This is a spatial feature which has a minor effect in the recognition of terrain. The second component is the MSS 4 band average of the cell.

• Original samples

○ Linearly interpolated samples along rows

+ New samples by row interpolation

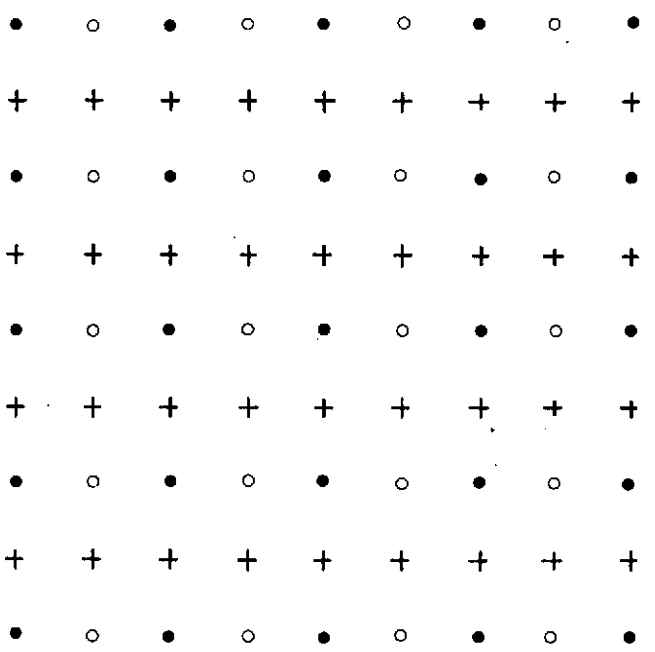

Fig. 3-3 — Fourier transform interpolation

The third component is the MSS 5 band average of the cell. The fourth component is the MSS 7 band average of the cell. The fifth component is the sum of the spatial features S_1, S_2, S_3 and S_4. The sixth component is the product of the spatial features S_1, S_2, S_3 and S_4. The seventh component is the ratio $(S_2 \cdot S_4)/(S_1 \cdot S_3)$.

It is possible that the interpretation results could be affected by changes in the amplitude levels of the features. In particular, the spatial features which are computed by integrating regions of the cell Fourier transforms experience amplitude variations as the cell size is changed. These variations are partially corrected by interpolating the Fourier transform so that it will contain at least 33 x 33 pixels before the spatial features are computed. In addition, two feature amplitude normalizations are executed before cell vectors are assigned to clusters. The first normalization occurs before the non-linear amplitude transformations have been applied and the second normalization after the non-linear transformations.

The need for the non-linear transformations was demonstrated in the first part of the investigation when the spatial features were found to be highly non-gaussian. Non-linear transformations applied to the feature space were developed to change the statistics of the terrain classes. A different transformation is required for each feature component.

The non-linear transformations that have been employed are power transformations such that

$$\begin{bmatrix} y_1 \\ \vdots \\ y_7 \end{bmatrix} = \begin{bmatrix} x_1^{\epsilon_1} \\ \vdots \\ x_7^{\epsilon_7} \end{bmatrix} \qquad (3\text{-}3)$$

where $x_1 \ldots x_7$ are the input feature components
$y_1 \ldots y_7$ are the output feature components
$\epsilon_1 \ldots \epsilon_7$ are the power exponents to which the corresponding input features are raised.

The exponents $\epsilon_1 \ldots \epsilon_7$ have been adjusted individually so that each output feature y_i would be approximately gaussian in all terrain classes. If the amplitudes of the input features vary substantially, then the power exponents may not be optimum. For this reason, the input features x_i are normalized before the non-linear transformation of Eq. (3-3) is applied. The normalization consists of determining the maximum and minimum values of a feature component x_i by

examining the input vectors. Let the difference between the maximum and minimum values be the range R_i. Then, the component x_i of each vector is multiplied by (K/R_i). Thus, after the normalization, the range of each feature component is the constant K.

After the non-linear transformations (Eq. 3-3), another normalization is applied to ensure that the proper weighting factors are employed for each feature component. In this case, the mean and standard deviation of each component over the vectors is computed. Then the ith component is normalized through multiplication by a factor (K_i/σ_i) where K_i is a selected constant and σ_i is the standard deviation of the ith component. After the normalization, the standard deviation of the ith component is K_i. The constants or weights K_i $(i = 1, 2, \ldots, 7)$ need not all be equal. By varying these constants, one can emphasize one feature component more than the others. The larger K_i, the greater the emphasis of the ith component. If K_i is larger than the other feature weights, the ith component tends to influence the clustering operation of vectors more than the remaining components.

The two amplitude normalizations were introduced to insure that the cell size would not produce feature amplitude variations which may reduce the effectiveness of the non-linear transformations. The adequacy of the normalizations was checked by computing histograms of feature components from 9 x 9 pixel cells. Training vectors were selected from cells of known terrain and were processed through both normalizations and the non-linear transformation. The histograms showed that the features were approximately gaussian and the amplitude normalizations were satisfactory.

3.3.2 Statistics of the Features

An insight into the effects of cell size on the features can be gained by examining the statistics of the feature vectors. For this purpose, the statistics of training vectors were computed. However, it is even more instructive to examine the statistics of cluster cores formed by the clustering program. Cluster cores were selected which contain vectors of a single terrain class. For each cluster core the mean vector was computed and the standard deviations of the core vectors from the mean vector. Let $m_1, m_2, \ldots m_7$ be the mean vector components and $\sigma_1, \sigma_2, \ldots \sigma_7$ be the standard deviations from the mean vector in the seven feature components.

$$m_i = \frac{1}{N} \sum_{j=1}^{N} x_{ij} \qquad i = 1, \ldots, 7 \qquad (3\text{-}4)$$

where x_{ij} = the ith component of the jth vector
N = the number of vectors in the cluster core.

$$\sigma_i^2 = \frac{1}{N} \sum_{j=1}^{N} (x_{ij} - m_j)^2 \qquad (3\text{-}5)$$

As the cell size is reduced, the mean vectors for each terrain class remain roughly constant. However, the standard deviations on the average increase, with decreasing cell size. This can be demonstrated by summing up the standard deviations for each terrain class. Furthermore, one may divide the sum of the standard deviations by the sum of the components of the mean vector, in order to normalize any remaining scale differences in the feature space. Thus, the parameter ρ is formed so that

$$\rho = \frac{\sum_{i=1}^{7} \sigma_i}{\sum_{i=1}^{7} m_i} \qquad (3\text{-}6)$$

Table 3-1 shows how the parameter ρ is affected by cell size. An increase in ρ implies that the cluster cores are becoming more diffuse. Table 3-1 shows that ρ consistently increases for all terrain classes as the cell size is reduced. The largest changes in ρ occur for the terrain categories of farms and mountains. In fact, in the following sections, it is shown that the mountains could not be identified as a separate terrain class for the smallest cell (9 x 9 pixels).

More insight into the effects of cell size can be gained by examining the divergence between cluster cores.

3.3.3 Divergence Between Cluster Cores

Divergence is a test of statistical separability between terrain classes in feature space. Let

$$L(X) = \frac{P_I(X)}{P_j(X)} \qquad (3\text{-}7)$$

Table 3-1.

Variations in the Parameter ρ with Cell Size

Terrain Class	Cell Size		
	17 x 17 pixels	13 x 13 pixels	9 x 9 pixels
Urban	$\rho = 0.0236$	$\rho = 0.0308$	$\rho = 0.0344$
Mountains	" = 0.0283	" = 0.0330	" = 0.0441
Desert	" = 0.0250	" = 0.0288	" = 0.0299
Farms	" = 0.0265	" = 0.0404	" = 0.0432

Urban	$*\Delta\rho = 0.0108$
Mountains	" = 0.0158
Desert	" = 0.0049
Farms	" = 0.0167

*$\Delta\rho$ is the difference in the parameter ρ between the 17 x 17 pixel cells and the 9 x 9 pixel cells.

Table 3-2.

Cluster Core Divergences

Pairs of Terrain Classes	17 x 17 Pixels	13 x 13 Pixels	9 x 9 Pixels
Urban-Mountains	350	79	58
Urban-Desert	1,178	535	1×10^{15}*
Urban-Farms	389	83	57
Mountains-Desert	550	182	6×10^{14}*
Mountains-Farms	734	351	226
Desert-Farms	3,510	1,989	3×10^{15}*

* Spurious values resulting from a component (the derivative count) which is consistently zero for the desert class.

where X is a feature vector

$P_i(X)$ = probability that vector X belongs to the ith class.

$P_j(X)$ = probability that vector X belongs to the jth class.

The divergence between classes i and j is defined as

$$D(i,j) = \oint \log L(X)\ Pi(X)\ dX - \oint \log L(X)\ Pj(X)\ dX \qquad (3\text{-}8)$$

For gaussian classes,

$$D(i,j) = \frac{1}{2}\ \text{Trace}\ (V_i - V_j)(V_j^{-1} - V_i^{-1}) + \frac{1}{2}\ (M_i - M_j)^T\ (V_i^{-1} + V_j^{-1})\ (M_i - M_j) \qquad (3\text{-}9)$$

where V_i is the covariance matrix of the ith class

V_i^{-1} is the inverse covariance matrix

M_i is the mean vector of the ith class.

The divergence is a distance measure between two classes. If the covariance matrices are equal ($V_i = V_j$), then

$$D(i,j) = (M_i - M_j)^T\ V_i^{-1}\ (M_i - M_j) \qquad (3\text{-}10)$$

If, in addition, $V_i = I$, the unity matrix then

$$D(i,j) = \sum_{k=1}^{7} (m_{ik} - m_{jk})^2 \qquad (3\text{-}11)$$

which is the square of the distance between the mean vectors.

If the divergence decreases as the cell size is reduced, then the two classes become statistically less distinguishable or separable. Table 3-2 shows the changes in divergences as the cell size is decreased. These divergence values have been computed from the statistics of the cluster cores.

Table 3-2 shows that the divergences between the various terrain classes decrease rapidly as the cell size is reduced. For the smallest cell size (9 x 9 pixels), a degenerate situation arose where one feature component (the derivative count) of the desert class was always zero and very large spurious divergence values resulted.

3.4 Terrain Recognition Accuracy versus Cell Size

Image 1031-17325 was divided into 3,360 cells of 17 x 17 pixels each. The cells are arranged in 56 rows by 60 columns. The vectors from these cells were processed through the clustering algorithm and the results are summarized in Table 3-3. This table should be compared with Table 3-4, which shows the interpretation results for the same image, but for a cell size of 32 x 32 pixels. Tables 3-5 and 3-6 summarize the clustering results for the same image and for cell sizes of 13 x 13 pixels and 9 x 9 pixels, respectively.

Examination of the above tables shows that as the cell size is reduced, the detection rates for the various terrain classes decrease and, in addition, the number of classes that can be clustered is reduced. For example, for the 9 x 9 pixel cells, mountains were not identified as a separate class, but instead were assigned to the desert and urban classes. The best detection rates were achieved with the 32 x 32 pixel cells; however, acceptable detection rates appear possible with 17 x 17 pixel cells.

Figures 3-4 through 3-6 show the MSS 5 band of image 1031-17325 with the clustering results superimposed as numerical connotation.

Table 3-3. Comparison of Clustering Results

ERTS-1 Image 1031-17325
Phoenix, Arizona

17 x 17 Pixels Cell Size

Computer	Photointerpreter B	U	M	D1	F	D2	R
0	89	21	36	0	26	69	7
1	0	313	12	0	14	14	50
2	0	5	316	0	3	39	11
3	0	0	0	88	0	0	0
4	0	18	7	0	738	27	13
5	0	32	59	0	52	1281	20

Detection Rates, %	
U	80
M	73
D1	100
F	89
D2	90

B = Boundaries
U = Urban
M = Mountains and Hills
D1 = Smooth Desert
F = Farms
D2 = Rough Desert
R = Riverbeds

Table 3-4. Comparison of Classification Results

ERTS-1 Image 1031-17325, Phoenix, Arizona

32 x 32 Pixels Cell Size

Class	D	F	M	U	R
1	429	0	6	0	6
2	1	407	0	10	7
3	31	0	114	0	1
4	1	1	3	57	11
Total	462	408	123	67	25

Detection Rates, %

D	93
F	100
M	93
U	85

D = Desert

F = Farms

M = Mountains

U = Urban

R = Riverbeds

Table 3-5. Comparison of Clustering Results

ERTS-1 Image 1031-17325
Phoenix, Arizona

13 x 13 Pixels Cell Size

Computer	Photointerpreter B	U	M	D	F	R
0	67	13	21	50	20	10
1	0	359	72	320	136	101
2	0	12	330	56	8	19
3	0	2	20	769	0	11
4	0	27	5	25	709	19

Detection Rates, %	
U	87
M	74
D	63
F	81

B = Boundaries
U = Urban
M = Mountains
D = Desert
F = Farms
R = Riverbeds

Table 3-6. Comparison of Clustering Results

ERTS-1 Image 1031-17325
Phoenix, Arizona

9 x 9 Pixels Cell Size

	Photointerpreter					
	B	U	D	F	M	R
0	33	8	5	20	2	3
1	0	352	251	176	245	113
2	0	24	1197	14	155	9
3	0	33	25	665	6	24

Detection Rates, %

U	84
D	81
F	76

B = Boundaries
U = Urban
D = Desert
F = Farms
M = Mountains
R = Riverbeds

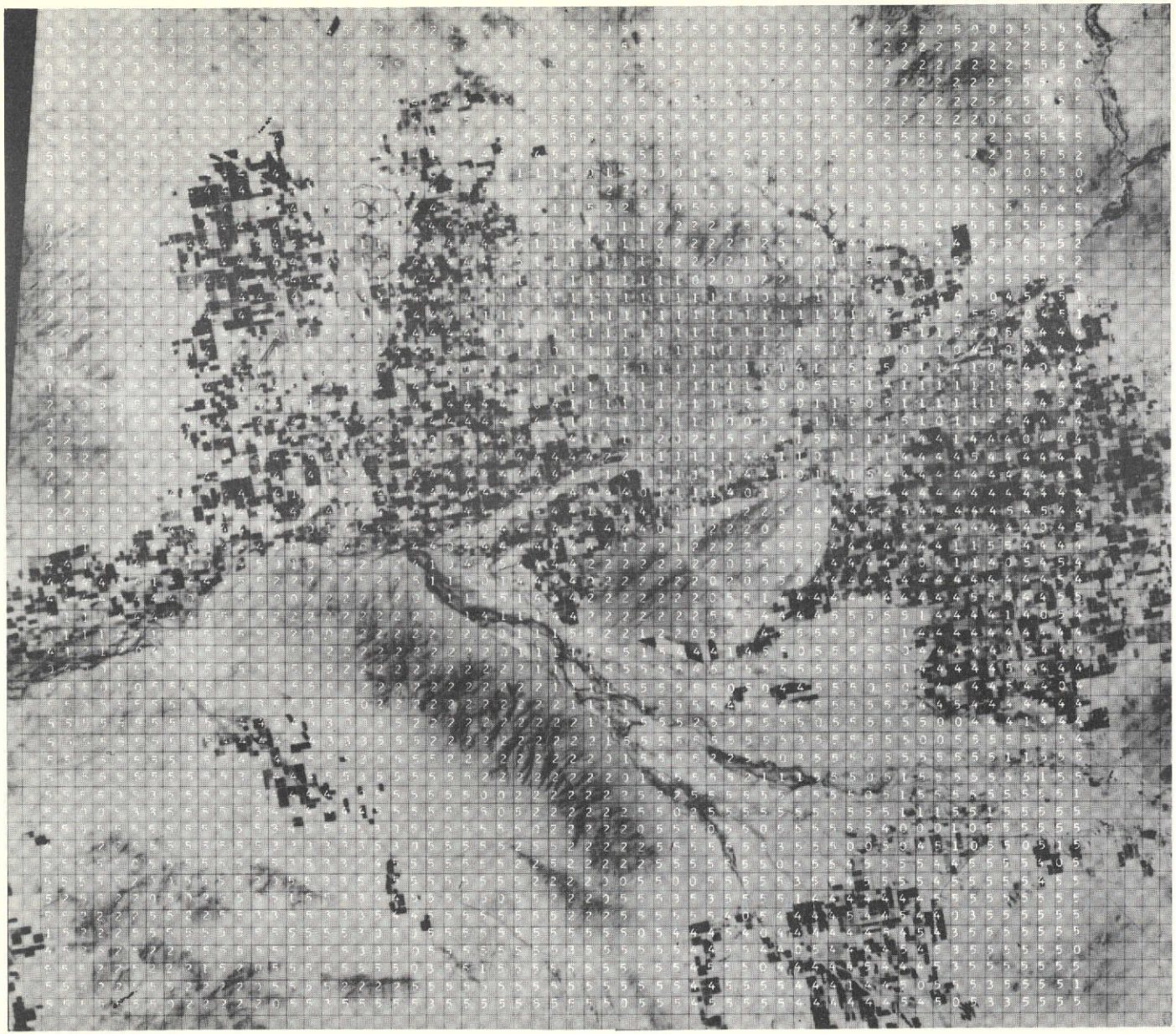

Fig. 3-4 — ERTS-1 image 1031-17325 (Phoenix, Arizona) with clustering results (17 × 17 pixel cells)

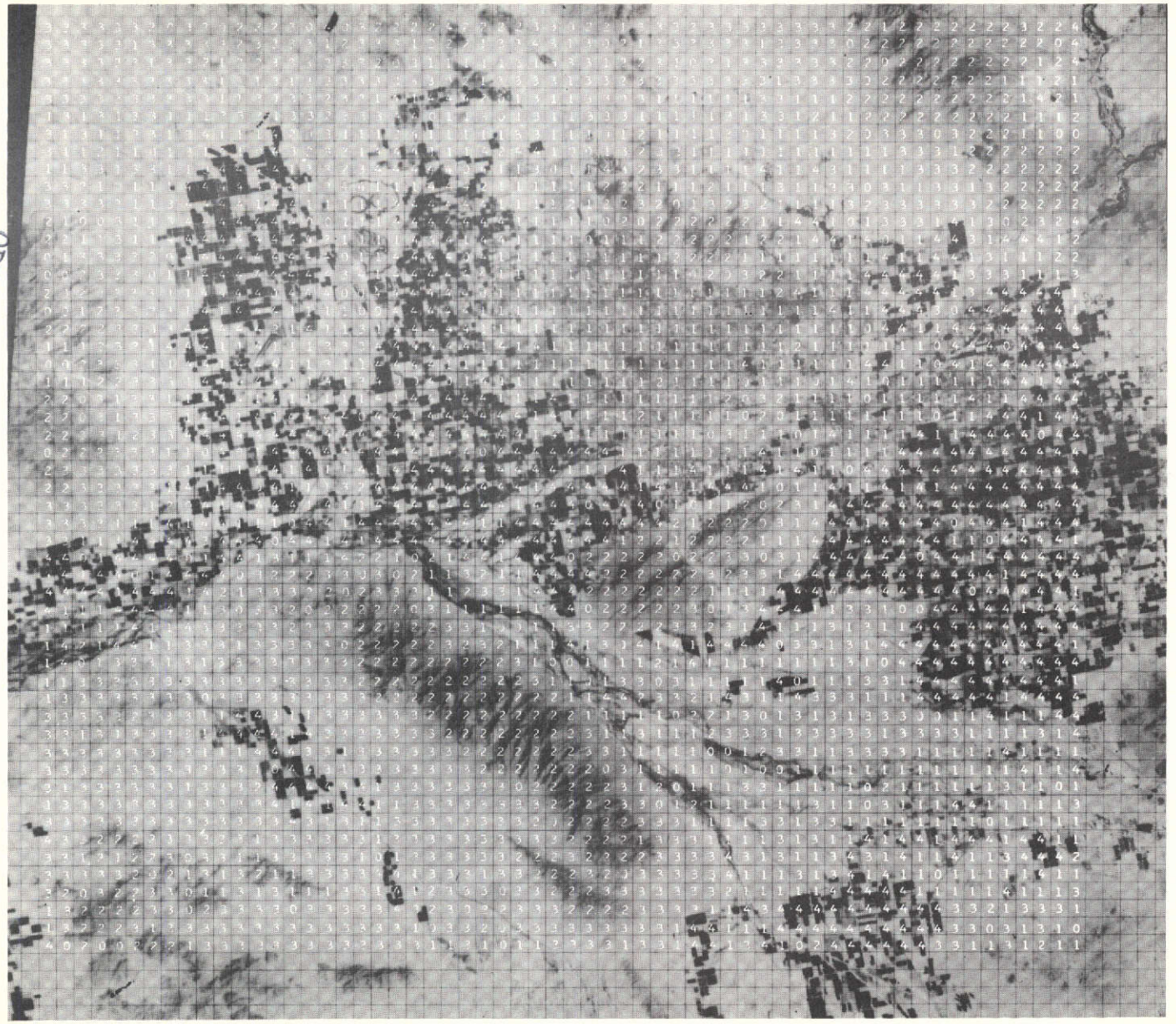

Fig. 3-5 — ERTS-1 image 1031-17325 (Phoenix, Arizona) with clustering results (13 × 13 pixel cells)

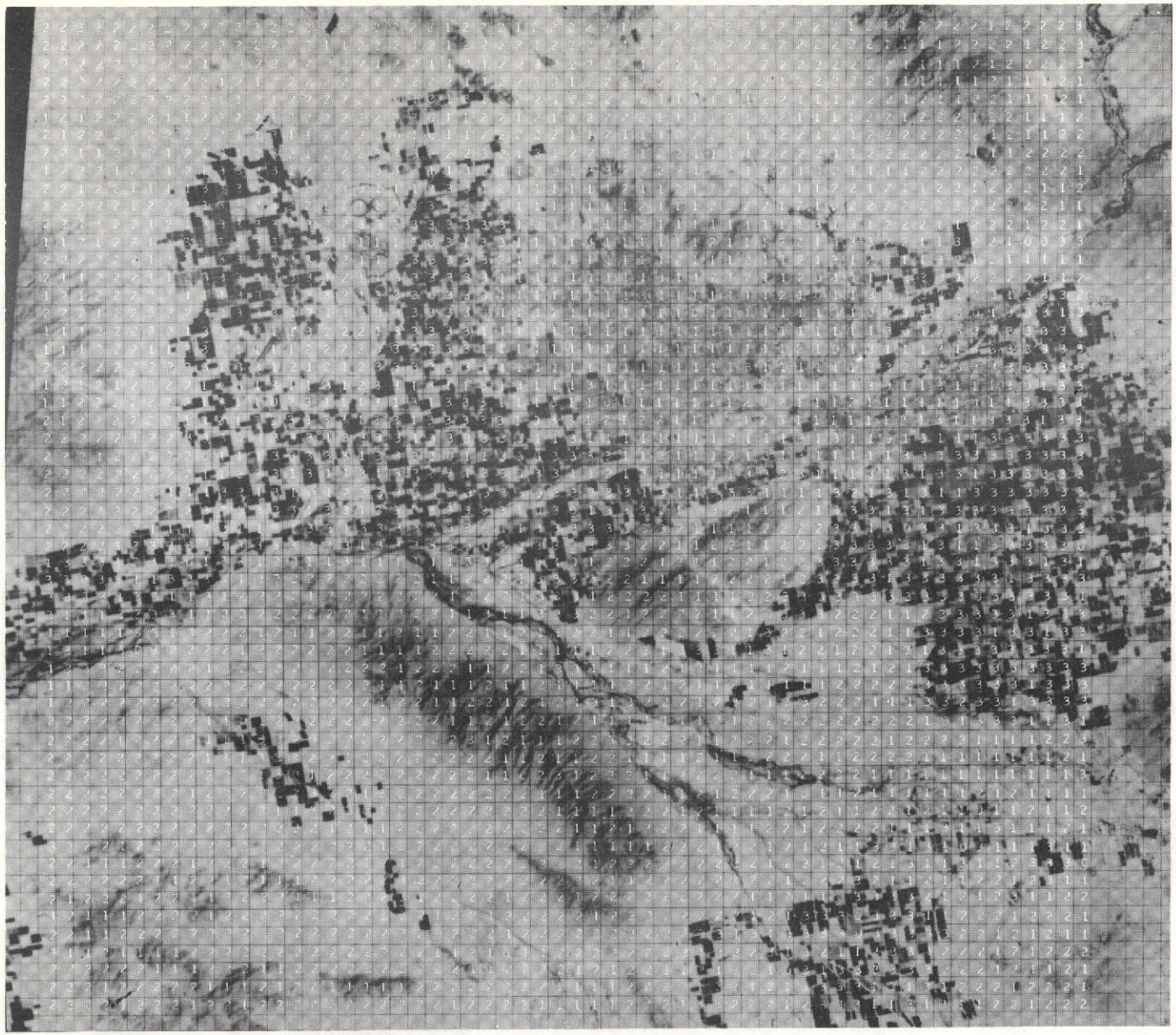

Fig. 3-6 — ERTS-1 image 1031-17325 (Phoenix, Arizona) with clustering results (9 × 9 pixel cells)

4. SECOND-LEVEL CLASSIFICATION RESULTS

At the beginning of the second part of this investigation, it was hoped that by reducing the cell size it might be possible to expand the number of terrain classes that can be recognized. For example, the urban area of Phoenix, Arizona could be determined with high accuracy using 32 x 32 pixels cells. Then, it was conceivable to break down the urban area into several classes such as industrial, commercial, residential, etc. by processing through the clustering algorithm vectors of smaller cell size such as 17 x 17 pixels or 9 x 9 pixels. This concept could be successful if there was one optimum cell size for separating the urban areas from non-urban terrain and a different optimum cell size for separating urban subclasses.

The results of Section 3 where the cell size effects on terrain recognition were examined in depth, disproved the idea of an optimum cell size. Instead of the detection rate of a terrain class peaking sharply at a certain cell size, one observes a steady decline in the detection rates as the cell size is reduced. The decrease in the detection rates coincides with a general decrease in the divergence values between any two terrain clusters in feature space, which, in turn, signifies that the clusters become diffuse as the cell size is reduced.

In order to test further the possibility of second level classification with small size cells, it was decided to divide image 1031-17325 into a grid of 17 x 17 pixel cells with adjacent cells touching each other so that each pixel was assigned to only one cell. As the cell size was reduced, it was important to associate each cell with a specific 17 x 17 pixels cell, so the original grid was retained. This grid consists of rows 18, 35, 52, etc. and columns 69, 86, 103, etc. The upper left corner of each cell is defined by the intersection of a grid row with a grid column. While the cell size was varied, the upper left corner of each cell was always the same. Thus, a 17 x 17 cell could be reduced to a 15 x 15 cell by eliminating its last two rows and last two columns. This approach guaranteed that a smaller cell was wholly contained within a larger cell and, in fact, it was the upper left corner of the larger cell. Of course, adjacent cells smaller than 17 x 17 pixels were no longer touching each other, but were separated by pixels not assigned to any cell. The advantage of this approach is that smaller cells can be directly related to larger cells and, therefore, the clustering algorithm assignments for any location on the ground can be identified as the cell size was changed.

A 17 x 17 pixel cell corresponds to an elementary area on the ground of 1.35 kilometers square. Such an area would be assigned to a cluster class for each cell size. Three cell sizes were processed through the clustering algorithm: 17 x 17

pixels, 13 x 13 pixels and 9 x 9 pixels. Hence, each elementary area was assigned to three terrain classes. It was hoped that more terrain classes could be recognized by cross-referencing the three terrain classes for each elementary area. This would have been possible if the smaller size cells provided additional information about an elementary area. Unfortunately, the smaller size cells have not contributed any new information that is not provided by the 17 x 17 pixel cells. Examination of Tables 3-3 through 3-6 and Figures 3-4 through 3-6 shows this to be the case.

In addition, the operation of the clustering algorithm was examined for clues which would indicate the kind of terrain information that might be provided by the smaller size cells. The most crucial part of the clustering algorithm is the formation of the cluster cores. Some of these cores are later eliminated if their divergence values from other cluster cores do not exceed a specified value. The initial cluster cores are formed before the divergence test is applied and indicate the kind of terrain information provided by the smaller size cells. When vectors from the 17 x 17 pixel cells were processed through the clustering algorithm, ten cluster cores were initially formed and are described in Table 4-1. This table shows that only mixed cluster cores were eliminated by the divergence test. When vectors from the 13 x 13 pixel cells were processed through the clustering algorithm, nine cluster cores were initially formed and are described in Table 4-2. Nine initial cluster cores were also formed when vectors from 9 x 9 pixel cells were processed. These cluster cores are described in Table 4-3. Examination of Tables 4-1 through 4-3 shows that the cluster cores become more mixed as the cell size is reduced. In addition, mountains and hills tend to appear together as a single class. In Table 4-3, cluster core number 4 could have developed into a mountains and hills cluster if its divergence values from the other cluster cores had been larger than the specified threshold. However, as described in Section 3.3.3, the divergence values have been decreasing with cell size and when the divergence of cluster core number 4 (for the 9 x 9 pixel cell size) fell below the threshold, a separate mountainous terrain cluster was not developed.

Since most of the cluster cores in Tables 4-1 through 4-3 contain vectors from diverse terrain types, it does not appear that additional terrain information can be obtained from the smaller cell sizes.

In Section 5, it is shown that it is possible to obtain a second-level classification by careful adjustment of the clustering algorithm thresholds using only 17 x 17 pixel cells. For example, in the Los Angeles area four separate urban classes, two separate mountain classes and a hill class were recognized by the clustering algorithm using 17 x 17 pixel cells.

Table 4-1. Initial Cluster Cores

17 x 17 Pixels Cell Size

Cluster Cores in the Sequence of Formation	Description of Cluster Vectors	Final Disposition after Divergence Test
1	100% Urban	Retained
2	100% Mountains	Retained
3	61% M, 39% H	Eliminated
4	100% Desert	Retained
5	100% Farms	Retained
6	44% U, 39% R, 11% F, 6% H	Eliminated
7	44% H, 39% R, 17% U	Eliminated
8	89% D, 6% R, 5% F	Retained
9	83% F, 11% U, 6% R	Eliminated
10	61% M, 33% H, 6% R	Eliminated

U = Urban

M = Mountains

H = Hills

R = Riverbeds

F = Farms

D = Desert

Table 4-2. Initial Cluster Cores

13 x 13 Pixels Cell Size

Cluster Cores in the Sequence of Formation	Description of Cluster Vectors	Final Disposition after Divergence Test
1	85% U, 12% F, 3% R	Retained
2	58% H, 38% M, 4% U	Retained
3	96% D, 4% R	Retained
4	31% R, 27% H, 4% D, 31% U, 7% M	Eliminated
5	31% R, 50% F, 19% U	Eliminated
6	58% M, 35% H, 7% R	Eliminated
7	100% Farms	Retained
8	55% R, 14% H, 14% U, 14% F, 3% D	Eliminated
9	34% H, 21% M, 21% U, 21% D, 3% R	Eliminated

U = Urban

R = Riverbeds

F = Farms

D = Desert

H = Hills

M = Mountains

Table 4-3. Initial Cluster Cores

9 x 9 Pixels Cell Size

Cluster Cores in the Sequence of Formation	Description of Cluster Vectors	Final Disposition after Divergence Test
1	81% U, 12% R, 7% F	Retained
2	89% D, 11% R	Retained
3	46% H, 15% U, 16% R, 15% F 4% M, 4% D	Eliminated
4	58% H, 35% M, 4% U, 3% D	Eliminated
5	96% F, 4% U	Retained
6	50% R, 16% H, 15% F, 15% U 4% D	Eliminated
7	50% M, 35% H, 15% R	Eliminated
8	33% F, 23% R, 27% U, 13% M, 4% H	Eliminated
9	27% D, 27% R, 20% U, 17% H, 6% F, 3% M	Eliminated

U = Urban

R = Riverbeds

F = Farms

D = Desert

H = Hills

M = Mountains

5. APPLICATIONS OF THE CLUSTERING ALGORITHM

In the first part of the investigation, it had been shown that major terrain types could be recognized with high accuracy using 32 x 32 pixel cells and the clustering algorithm developed by this investigation. In the second part of the investigation, it is shown (see Section 3) that major terrain types can be recognized with good accuracy using 17 x 17 pixel cells. ERTS data from five geographical regions of the United States were processed through the clustering algorithm using 17 x 17 pixel cells. The results provide additional tests of this cell size and of the clustering algorithm and offer a basis of comparison with the results obtained by other investigators.

Data from the following ERTS images was processed:

1090-18012 from Los Angeles, California.
1080-15192 from Washington, D. C.
1273-18183 from San Francisco, California.
1258-15082 from New York, New York.
1376-17452 from Hill County, Montana.

5.1 Los Angeles Area

ERTS image 1090-18012 over the Los Angeles area was acquired on October 21, 1972. Data from this image has been processed repeatedly through the clustering algorithm with different algorithm parameters in an effort to optimize the clustering algorithm. When 32 x 32 pixel cells are used, the clustering algorithm produces excellent results and it is not necessary to fine tune its parameters. However, the 17 x 17 pixel cells produce cluster cores that are less separable statistically and the clustering algorithm must be fine tuned to produce the best possible interpretation results.

5.1.1 Clustering Algorithm Operation

Figure 5-1 shows a block diagram of the clustering algorithm that has been developed. In the first subroutine (Distance Computation) an Euclidean distance is computed for every pair of vectors. About 400 vectors are inputed and 79,800 distances between them are computed. The distances are compared to an initial threshold t_o and those smaller than t_o are stored together with the vectors that produced them. This operation should produce a list of 600-800 minimum distances. If fewer than 600 distances are found, the threshold t_o is increased. All the distances are computed again, and those less than the new threshold are stored.

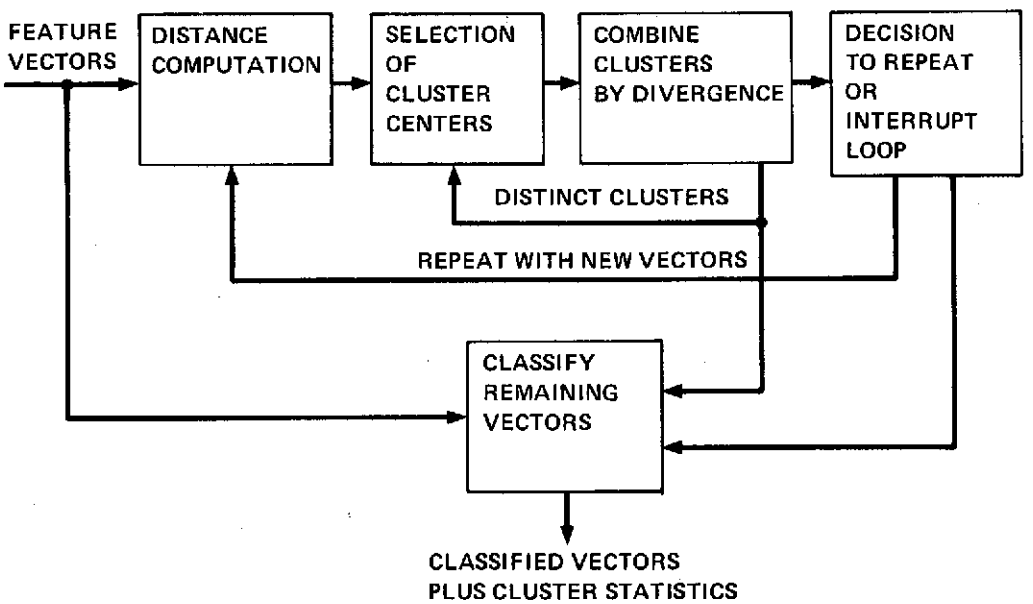

Fig. 5-1 — Clustering algorithm block diagram

Conversely, if more than 900 distances are found, then the threshold is reduced, etc. One of the algorithm parameters that has been varied is the number of minimum distances that are retained. This parameter was varied between 600 and 1,400 and is identified by the letters, NDD.

In the next subroutine (Selection of Cluster Centers), the input data consists of the 600 minimum distances and two vector arrays containing the vectors associated with these distances. A search is made through these vector arrays, and all vectors (V_j) which appear more than 15 times are identified as potential centers of clusters. For each vector V_j, the distances d_{jk} from the associated V_k vectors are listed and ordered in increasing magnitude. The 16 smallest distances are summed and form the sums S_{jk}. Assuming there were twelve vectors V_j, there will be twelve sums S_{jk}. The minimum of these is selected, and the associated vector $(V_j)m$ is selected as the center of the densest cluster. All vectors V_k associated with $(V_j)m$, are assigned to the first cluster. This operation leads to the formation of the core of cluster no. 1 which is also the densest cluster. Note that a specific vector may belong to the V_j category by appearing more than 15 times and the V_k category by being associated with another vector V_j. Therefore, all vectors which are assigned to cluster no. 1 are subsequently removed from the V_j and the V_k categories. This guarantees that subsequent clusters to be formed will not overlap with cluster no. 1. Of the original set of twelve V_j vectors, there may remain only five vectors after the no. 1 cluster vectors are removed. Seven V_j vectors were eliminated either because they were assigned to cluster no. 1 or because they lost some of their V_k vectors to cluster no. 1 so they no longer had more than 15 vectors associated with them.

The reduced sets of V_j and V_k vectors are recycled through the same subroutine as if they were the original sets and the no. 2 cluster core is formed. Then, the V_j and V_k vector sets are reduced again and recycled through the same subroutine to form perhaps the core of cluster no. 3, etc. When no more V_j vectors are left, the formed clusters (three in this case) are tested in the next subroutine (Combine Clusters by Divergence) for statistical separability. The divergence between every pair of clusters is computed, and a pair of clusters is merged if the respective divergence value is less than 10. Such clusters tend to be adjacent parts of a larger cluster and should, therefore, be united. The clusters that survive this test, (perhaps two clusters are left in the examples given above) are the cores of the densest clusters. By eliminating them, it will then be possible to identify the less dense or diffuse clusters. Therefore, the entire sequence of processing operations is repeated except that the vectors

already assigned to clusters are not included in the input vector set. This clustering sequence produces a few more clusters, and the vectors assigned to those clusters are removed from the input vector set. A third recycling through the clustering algorithm usually terminates the cluster core formation by depleting the initial set of input vectors. Of the original 400 vectors, about 160 are assigned to about 10 elementary clusters. These elementary clusters consist of the cores of the dense and diffuse clusters, as well as regions of the vector space where vectors from two or more true clusters are intermixed. These false cluster cores are usually formed after the diffuse cluster cores. But, one does not know whether the last clusters to be formed are true or false. In other words, the clustering program will occasionally overproduce cluster cores.

Another parameter of the clustering algorithm that was varied is the minimum number of vectors required in each elementary cluster. This parameter identified by the letters NT has been varied between 15 and 25.

The false cluster cores are identified with a divergence test. The divergences of the last cluster to be formed against the other clusters are computed. If one or more divergence values are less than 45, the last cluster is dissolved. The same test is applied to the next to the last cluster, etc., so that all clusters retained have divergence values between each other, greater than 45. The result may be that from the 10 elementary clusters only a few (usually 3-8) are retained.

A third parameter that has been varied is the limit in the divergence test that the elementary clusters must pass in order to be retained. This parameter identified by the letters TD2 has been varied between 35 and 45.

At this point, the true cluster cores have been identified, but the cluster statistics are not known accurately and only about 100 vectors have been classified. In the last subroutine (Classify Remaining Vectors), the remaining vectors are assigned to the cluster cores by the maximum likelihood criterion. The assignment is done iteratively by first assigning vectors only near the cluster cores. Then, the cluster statistics are recomputed and additional vectors are assigned. In the process, the clusters grow and their statistics change. This subroutine allows for seven iterations. By the last iteration, most of the vectors have been classified. The remaining vectors are left in the unknown category (Class 0) because their probabilities of belonging to any cluster are very small.

Two more parameters are employed in this part of the algorithm and control the growing process of the clusters. The algorithm requires that the natural logarithm of the probability density that a given vector belongs to a specific cluster be larger than a threshold limit TC. This assures that no vector is assigned to a cluster unless it is located "near" the cluster center. The "nearness" is determined by the logarithm of the probability density which must exceed TC. TC was varied between (-20) and (-70) with the (-20) value being the most restrictive and causing the slowest assignment of vectors to the clusters.

In addition, the algorithm also requires that a vector cannot be assigned to a cluster if it is also "close" to another cluster. This is done to avoid erroneous assignments of vectors located in regions of the feature space which may be considered as border regions between clusters. Initially, the statistics of the final clusters are not known and the elementary clusters grow at different rates. Therefore, the borders between the clusters shift as the clusters grow. The test of "closeness" performed by the algorithm avoids the assignment of vectors located in the border regions before the clusters are fully grown. This test operates as follows:

a. Given a specific vector, the logarithms of probability densities of the vector belonging to each cluster are computed.

b. The vector would normally be assigned to the cluster for which the logarithm of the probability density is maximum. This assignment is rejected if the maximum logarithm value does not exceed the TC threshold mentioned above. If the TC threshold is exceeded, then the ratios of the maximum logarithm to the other logarithms are formed. Since the logarithms are negative numbers, the ratios are numbers between 0 and 1.

c. The "closeness" test requires that all the ratios of the maximum logarithm to the other logarithms be less than a selectable threshold TR, otherwise the vector is not assigned to any cluster. This test can be made more restrictive by shifting the threshold TR towards zero or more liberal by shifting TR toward unity. TR was varied between 0.50 and 0.85.

The logarithm of the probability density function is equivalent to the square of a normalized distance from the cluster center. Therefore, both tests effectively establish boundary surfaces around each cluster. The vectors assigned to a cluster are required to lie within the volume contained by the boundary surfaces of the cluster. Vectors not lying within the specified cluster volumes are left in the unassigned category. When the vectors have been exhausted (either assigned to clusters or left in the unassigned category), the cluster statistics are recomputed and the unassigned vectors are tested again. In each iteration, new vectors are added at the periphery of each cluster and the cluster grows. A cluster's growth is evident whenever its statistics are recomputed. Due to the new statistics, the boundary surfaces associated with the TC and TR thresholds expand as the cluster grows. The two thresholds obviously influence the assignment of vectors to the clusters and, therefore, the rate of growth of the clusters. If the rate of growth is too slow, the clustering process ends with a very large number of unassigned vectors. If the rate is very rapid, the clusters grow abnormally because vectors are assigned to clusters a lot faster than the cluster statistics are updated. As a result, some clusters grow at the expense of other clusters and many vectors may be erroneously assigned.

In order to achieve the best possible results, the thresholds of the clustering algorithm described in this section must be carefully adjusted.

5.1.2 Processing Results

Image 1090-18012 was processed repeatedly as we attempted to optimize the clustering results by adjusting the thresholds described in the previous section. These processing operations are summarized in Table 5-1. Operation no. 1 used the threshold values that had been established for the 32 x 32 pixel cells and produced four clusters. It appeared that the spectral features were de-emphasized and that more than four clusters could be produced by adjustment of the thresholds. Operation nos. 2, 3 and 4 were attempts to emphasize the spectral features, achieve more equal feature normalizations and improve the cluster growth characteristics. Abnormal cluster growth is usually characterized by slow cluster growth initially followed by very rapid growth towards the end of the vector assignment process. In addition, some clusters grow at the expense of others and a lot of vectors remain unassigned in the zero category.

Operation nos. 5 through 20 were attempts to increase the number of final clusters and improve the cluster growth process. More initial clusters can be formed by increasing the numbers of minimum distances (NDD) and reducing the required number (NT) of vectors per cluster core. NDD was increased in some

Table 5-1. Summary of Processing
Operations on Image 1090-18012, Los Angeles, California

Operation Number	Thresholds*	No. of Zeros	No. of Clusters	Comments
1	NDD = 600 NT = 15 TD2 = 45 TC = -70 TR = 0.75	198	A.† 11 B.‡ 4	Too few final clusters, and somewhat insensitive to spectral features.
2	NDD = 600 NT = 15 TD2 = 45 TC = -70 TR = 0.75	1278	A. 10 B. 6	Spectral features were emphasized. Too many zeros and the clusters grow too fast.
3	NDD = 600 NT = 15 TD2 = 45 TC = -50 TR = 0.50	1371	A. 11 B. 4	Clusters grow too fast. Too many zeros.
4	NDD = 600 NT = 15 TD2 = 45 TC = -50 TR = 0.50	953	A. 8 B. 3	Vectors from water regions intentionally removed to observe their effect on feature normalization. Clusters grow too fast. Too many zeros.
5	NDD = 800 NT = 20 TD2 = 45 TC = -20 TR = 0.50	1260	A. 6 B. 4	Clusters grow too fast. Too many zeros.

* See Section 5.1.1 for description of thresholds.

† Initial cluster cores formed before divergence test.

‡ Final cluster cores after divergence test.

Table 5-1. (Continued)

Operation Number	Thresholds	No. of Zeros	No. of Clusters	Comments
6	NDD = 800 NT = 17 TD2 = 45 TC = -70 TR = 0.50	232	A. 8 B. 4	Few final clusters. Abnormal cluster growth.
7	NDD = 600 NT = 15 TD2 = 45 TC = -70 TR = 0.75	76	A. 6 B. 3	Few final clusters. Abnormal cluster growth.
8	NDD = 800 NT = 15 TD2 = 45 TC = -25 TR = 0.75	128	A. 6 B. 4	Few final clusters. Abnormal cluster growth.
9	NDD = 800 NT = 15 TD2 = 45 TC = -60 TR = 0.75	149	A. 7 B. 4	Few clusters. Abnormal cluster growth.
10	NDD = 1200 NT = 17 TD2 = 45 TC = -65 TR = 0.85	104	A. 9 B. 3	Few clusters. Abnormal cluster growth.
11	NDD = 900 NT = 15 TD2 = 45 TC = -60 TR = 0.50	214	A. 10 B. 5	Abnormal cluster growth.

Table 5-1. (Continued)

Operation Number	Thresholds	No. of Zeros	No. of Clusters	Comments
12	NDD = 600 NT = 12 TD2 = 45 TC = -40 TR = 0.75	194	A. 10 B. 7	Abnormal cluster growth.
13	NDD = 1000 NT = 15 TD2 = 45 TC = -60 TR = 0.65	54	A. 11 B. 3	Few final clusters. Abnormal cluster growth.
14	NDD = 600 NT = 15 TD2 = 45 TC = -25 TR = 0.50	122	A. 6 B. 3	Few final clusters. Abnormal cluster growth.
15	NDD = 600 NT = 15 TD2 = 45 TC = -30 TR = 0.50	122	A. 6 B. 3	Few final clusters. Abnormal cluster growth.
16	NDD = 800 NT = 12 TD2 = 20 TC = -60 TR = 0.60	311	A. 10 B. 10	Normal cluster growth. Incomplete processing run.
17	NDD = 800 NT = 17 TD2 = 25 TC = -75 TR = 0.60	200	A. 6 B. 5	Few final clusters. Normal cluster growth.

Table 5-1. (Continued)

Operation Number	Thresholds	No. of Zeros	No. of Clusters	Comments
18	NDD = 600 NT = 12 TD2 = 45 TC = -60 TR = 0.75	308	A. 10 B. 9	A good clustering operation. Slightly restrictive cluster growth.
19	NDD = 700 NT = 13 TD2 = 45 TC = -65 TR = 0.80	184	A. 7 B. 4	Few final clusters. Abnormal cluster growth.
20	NDD = 700 NT = 14 TD2 = 45 TC = -65 TR = 0.85	218	A. 6 B. 4	Few final clusters. Abnormal cluster growth.
21	NDD = 600 NT = 12 TD2 = 45 TC = -65 TR = .85	478	A. 10 B. 9	Good Clustering Operation.
22	NDD = 600 NT = 12 TD2 = 60 TC = -65 TR = .85	393	A. 10 B. 7	Good Clustering Operation.

operations to 700, 800, 900, 1,000 and 1,200 distances to allow more vectors to be considered in the formation of the densest cluster cores. NT was also varied between 12 and 20. Finally, the best results were obtained in operation nos. 21 and 22 with NDD = 600 and NT = 12. The divergence threshold TD2 was kept at 45 for most operations except nos. 16 and 17, for which the threshold was reduced in order to increase the number of clusters that were retained. In operation no. 22, TD2 was increased to 60 in order to retain the more statistically distinct clusters.

In operation nos. 21 and 22, thresholds TC and TR are nearly the same as in operation no. 1. TC = -65 is a more restrictive test in the assignment of vectors to a cluster than TC = -70. On the other hand, TR = 0.85 is more liberal than TR = 0.75 in allowing vectors to be assigned to clusters.

The minor readjustments of the thresholds were necessary due to the changes in feature statistics resulting from the 17 x 17 cell size. It is reassuring that after the extensive parametric evaluation of the clustering algorithm (summarized in Table 5-1) the optimum thresholds are only slightly different than the optimum thresholds of the 32 x 32 cell size.

Tables 5-2 and 5-3 summarize the clustering results for operation nos. 21 and 22. In Table 5-2, four urban classes, two water classes and two mountain classes were recognized. It appears that classes 2, 4 and 5 represent the downtown areas of Los Angeles characterized by highways, office and commercial buildings. Class 3 consists of urban areas with some vegetation. Class 8 consists of mountains whose vegetation appears burnt, possibly damaged by smog. This class also includes some canyons and mountain slopes which appear dark due to solar elevations. Class 7 consists of the high mountains with healthy vegetation. Class 9 consists mainly of hills. The detection rate for hills appears low (37%) because many hills have also been assigned to classes 7 and 8. This does not necessarily indicate poor clustering performance because the photointerpreter distinguished hills from mountains on the basis of altitude, while the clustering algorithm classified on the basis of the spectral and spatial features which are not uniquely related to altitude. For example, certain mountain ridges due to their location receive little moisture and are relatively barren, so they appear similar to barren hills in a different location.

In Table 5-3, two classes were eliminated by a more stringent divergence test, so that only two urban classes (2 and 3) were recognized. The mountain and hill classes are essentially the same as in Table 5-2. The equivalence relationship is established by adding the number 2 to each class of Table 5-3. For example, class 5 in Table 5-3 is equivalent to class 7 of Table 5-2, etc.

Figures 5-2 and 5-3 show the MSS 5 band of image 1090-18012 with the interpretation results superimposed as numerical annotation.

Table 5-2. Comparison of Clustering Results

ERTS-1 Image 1090-18012, Los Angeles, California
Operation No. 21 of Table 5-1

Photointerpreter

Computer	B	W1	U1	U2	U3	U4	W2	M1	M2	H	C	F	S
0	90	1	← 115 →				0	← 95 →		68	4	5	0
1	0	13	0	0	0	0	0	0	0	0	0	0	0
2	0	0	106	0	0	0	0	0	0	0	0	1	0
3	0	0	0	429	0	0	0	← 2 →		4	0	15	0
4	0	0	0	0	327	0	0	← 5 →		8	0	2	0
5	0	0	0	0	0	203	0	← 16 →		10	4	2	0
6	0	0	0	0	0	0	36	0	0	0	0	0	0
7	12	0	← 31 →				2	574	0	104	16	2	3
8	1	0	← 5 →				0	0	307	88	3	0	0
9	0	0	← 58 →				0	← 23 →		168	1	1	0

B = Boundaries

W1, W2 } Two Water Classes

U1, U2, U3, U4 } Four Urban Classes

M1, M2 } Two Mountain Classes

H = Hills

C = Clouds

F = Farms

S = Snow

Detection Rates, %

W1	93
W2	95
All U	84
All M	86
H	37

Table 5-3. Comparison of Clustering Results

ERTS-1 Image 1090-18012, Los Angeles, California
Operation No. 22 of Table 5-1

Computer	Photointerpreter B	W1	U1	U2	W2	M1	M2	H	C	F	S
0	78	1	168		0	101		43	0	2	0
1	0	16	0	0	0	0	0	0	0	0	0
2	0	0	206	0	0	0	0	1	0	0	0
3	0	0	0	836	0	17		14	2	23	0
4	0	0	12		35	0	0	0	3	0	0
5	0	2	41		5	595	0	68	14	0	3
6	0	0	11		1	0	294	104	1	0	0
7	0	1	125		0	0	32	185	18	2	0

B = Boundaries

W1, W2 } Two Water Classes

U1, U2 } Two Urban Classes

M1, M2 } Two Mountain Classes

H = Hills

C = Clouds

S = Snow

F = Farms

Detection Rates, %

W1	80
W2	85
All U	74
All M	86
H	46

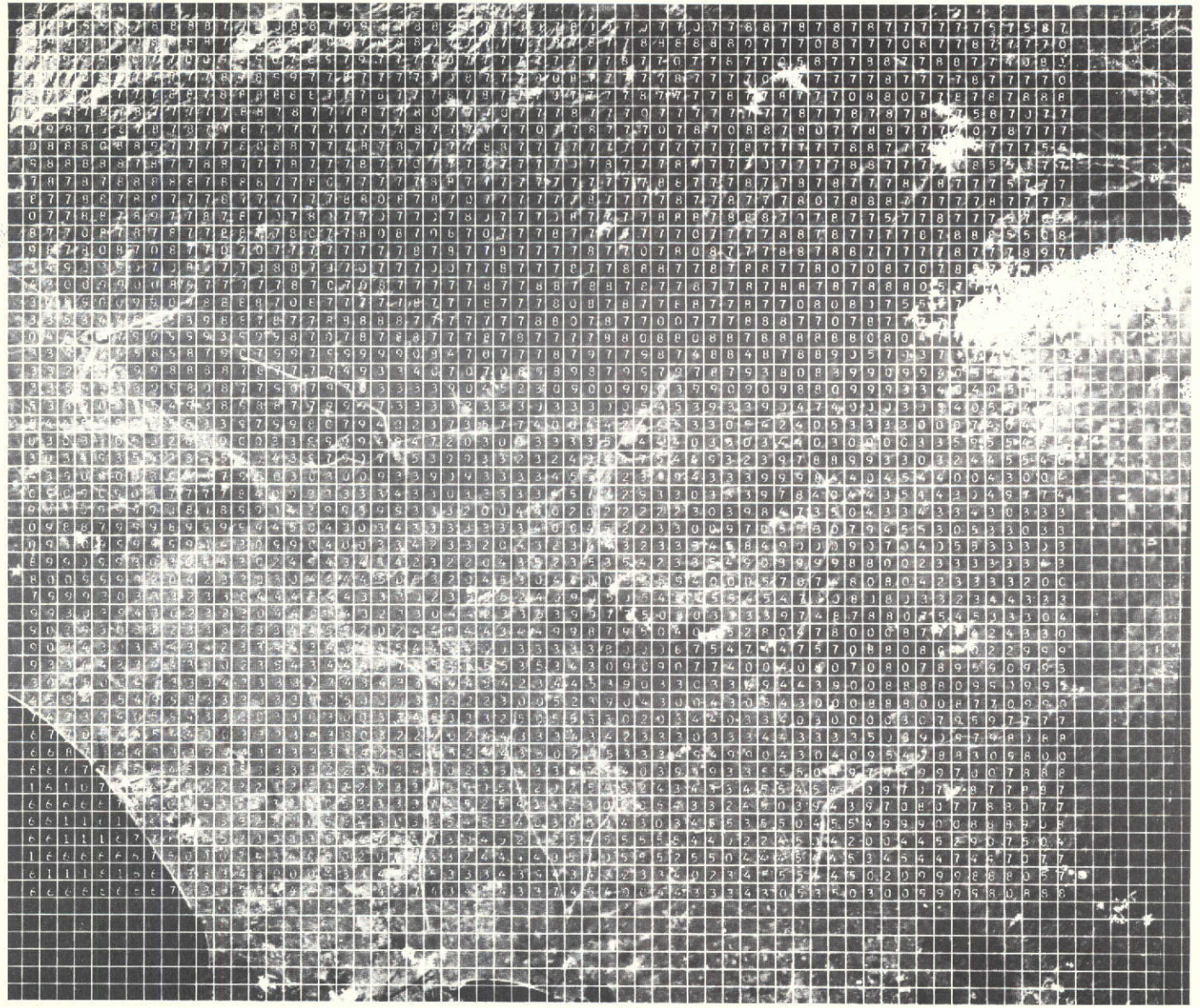

Fig. 5-2 — ERTS-1 image 1090-18012 (Los Angeles, California) with clustering results—operation no. 21 of Table 5-1

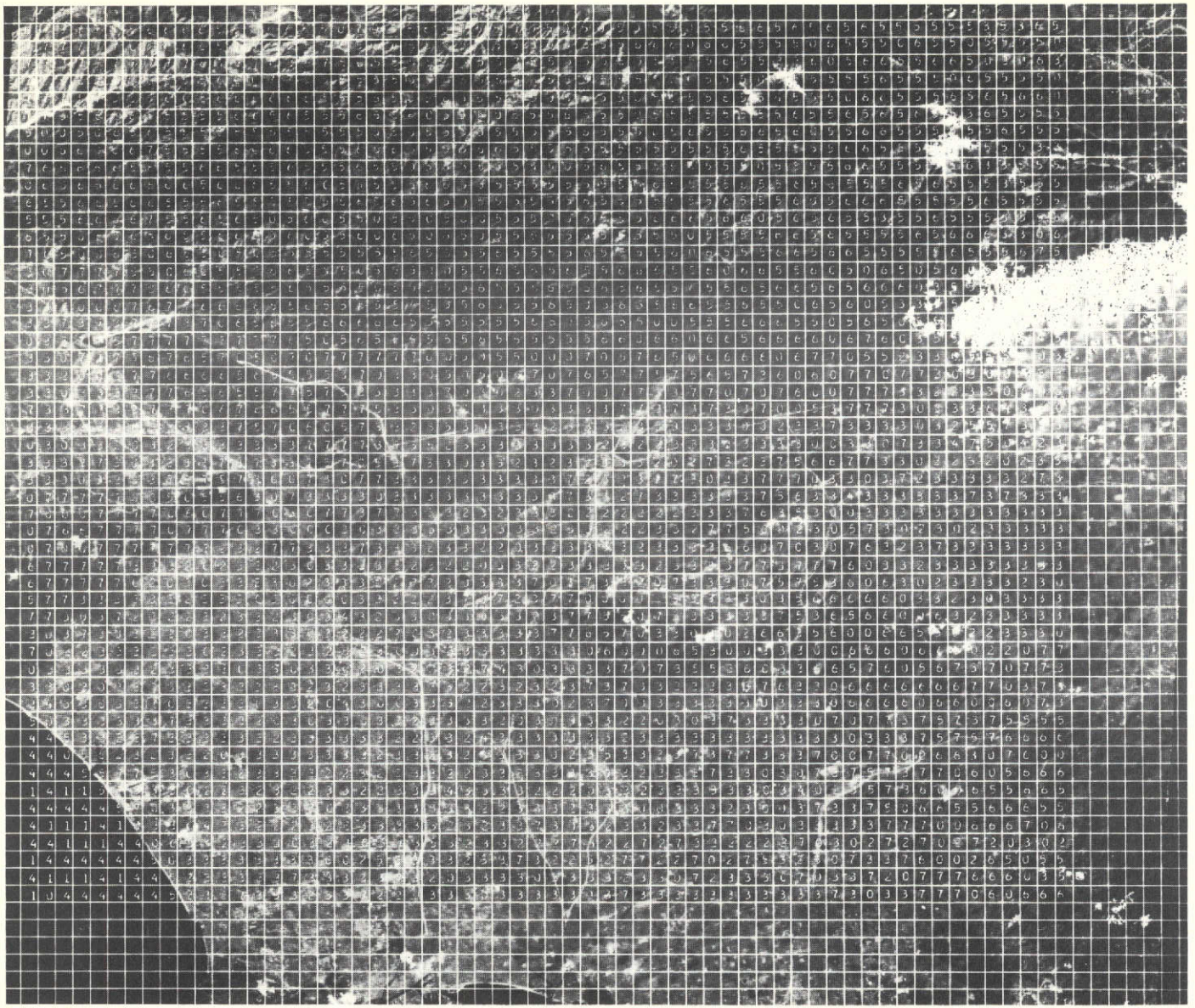

Fig. 5-3 — ERTS-1 image 1090-18012 (Los Angeles, California) with clustering results—operation no. 22 of Table 5-2

5.2 Washington, D.C. Area

ERTS-1 image 1080-15192 from the Washington, D. C. area was processed six times through the clustering algorithm. The purpose of these processing operations summarized in Table 5-4 is to adjust the thresholds for optimum clustering results. Operation nos. 5 and 6 gave the best results. The first two thresholds NDD and NT control the formation of the initial cluster cores (13 in operation no. 5, and 14 in operation no. 6). The divergence threshold TD2 reduces the final cluster cores to 7 and 8, respectively. The thresholds TC and TR control the cluster growth and the number of remaining unassigned vectors (the zeros).

The clustering results were photointerpreted, but a large number of photointerpreter errors were found because the Washington, D. C. area at the ERTS image scale is very confusing. This area is heavily wooded and flat with small farm plots. It is very difficult to distinguish the location of highways and the boundaries between farms, wooded areas and urban sections. The easily discernible terrain consists of the Potomac River, the Chesapeake Bay and the downtown sections of Washington and Baltimore. The clustering results are superimposed as numerical annotation of the MSS 7 image and shown in Figures 5-4 and 5-5, respectively. In Figure 5-4, class 1 is the Chesapeake Bay. Class 2 seems to represent valleys or low lands with rivers or lakes. The major concentration of class 2 vectors is in the Potomac River valley northwest of Washington, D. C. Class 3 is identified primarily with the coastal low lands of Maryland. It appears that class 3 is identified with heavily wooded areas. Class 4 signifies the downtown urban areas of Washington and Baltimore. Class 5 is identified by the residential urban areas around Washington and Baltimore. Classes 6 and 7 seemed to be the rural areas near the residential class which have not yet been substantially disturbed by urban expansion.

In Figure 5-5, two water classes in the Chesapeake Bay (classes 1 and 4) were recognized. Classes 2 and 3 appear to correspond to classes 2 and 3 of Figure 5-4. Class 5 is identified with urban areas. Class 6 also depicts urban areas which include major highway arteries. Class 7 is also an urban class. Class 8 depicts heavily forested areas.

5.3 San Francisco Area

ERTS-1 image 1273-18183 was also processed through the clustering algorithm using 17 x 17 pixel cells. This image depicts the city of San Francisco, the Bay area and a large part of the California Central Valley. The data processed through the clustering algorithm was entirely from the Central Valley around Stockton, California.

Table 5-4.
Summary of Processing Operations on Image 1080-15192
Washington, D.C. Area

Operation Number	Thresholds*	No. of Zeros	No. of Clusters	Comments
1	NDD = 800 NT = 17 TD2 = 45 TC = -25 TR = 0.75	175	A.† 7 B.‡ 3	Too few clusters. Abnormal cluster growth.
2	NDD = 800 NT = 15 TD2 = 45 TC = -60 TR = 0.75	320	A. 13 B. 7	Abnormal cluster growth.
3	NDD = 600 NT = 13 TD2 = 60 TC = -65 TR = 0.85	255	A. 14 B. 5	Abnormal cluster growth.
4	NDD = 600 NT = 14 TD2 = 60 TC = -65 TR = 0.85	278	A. 11 B. 6	Fair cluster growth.
5	NDD = 800 NT = 15 TD2 = 45 TC = -65 TR = 0.85	390	A. 13 B. 7	Good clustering results.
6	NDD = 600 NT = 13 TD2 = 45 TC = -65 TR = 0.85	53	A. 14 B. 8	Good clustering results.

* See Section 5.1.1 for description of thresholds.

† Initial cluster cores formed before divergence test.

‡ Final cluster cores after divergence test.

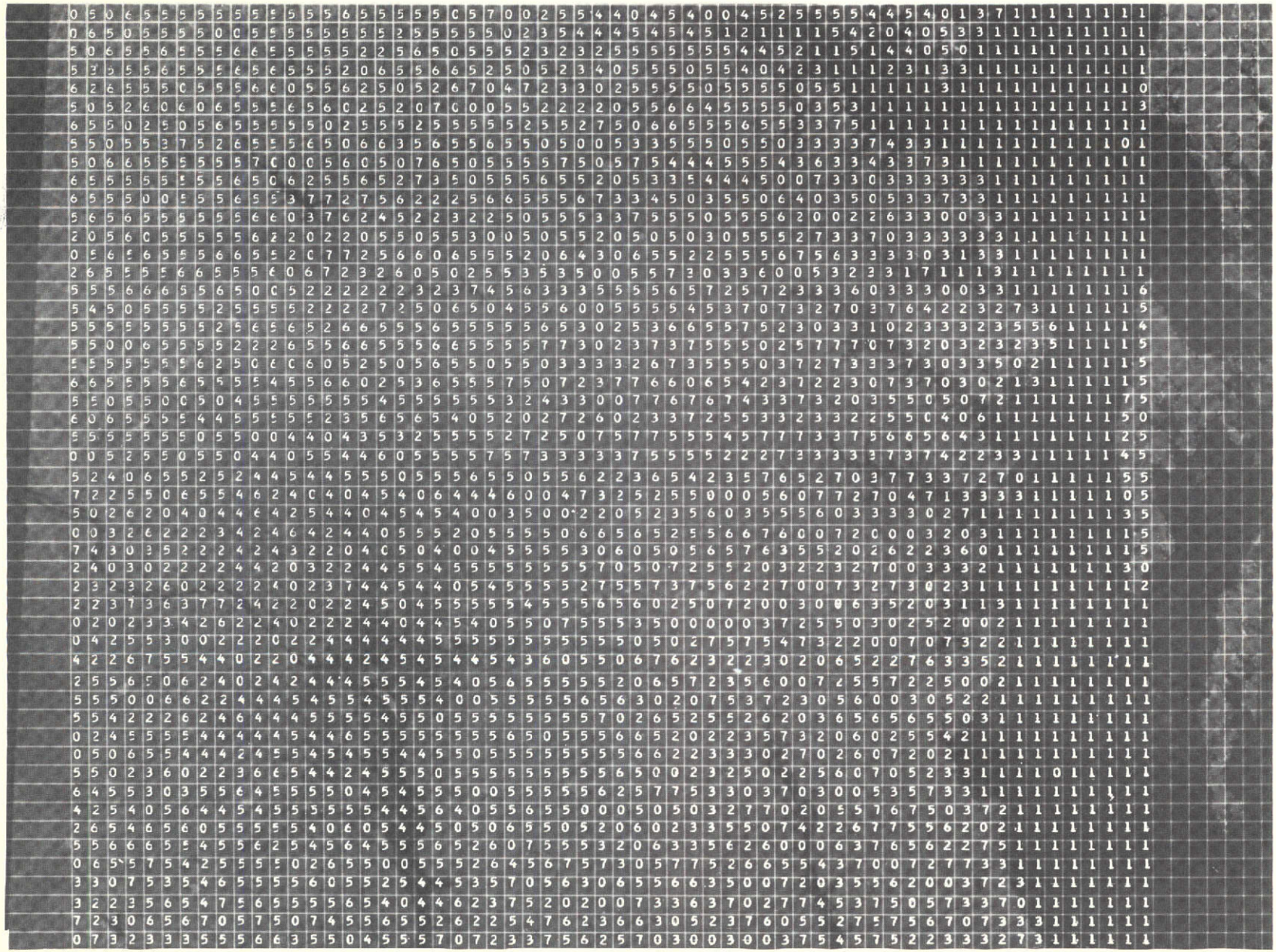

Fig. 5-4 — ERTS-1 image 1080-15192 (Washington, D.C.) with clustering results—operation no. 5 of Table 5-4

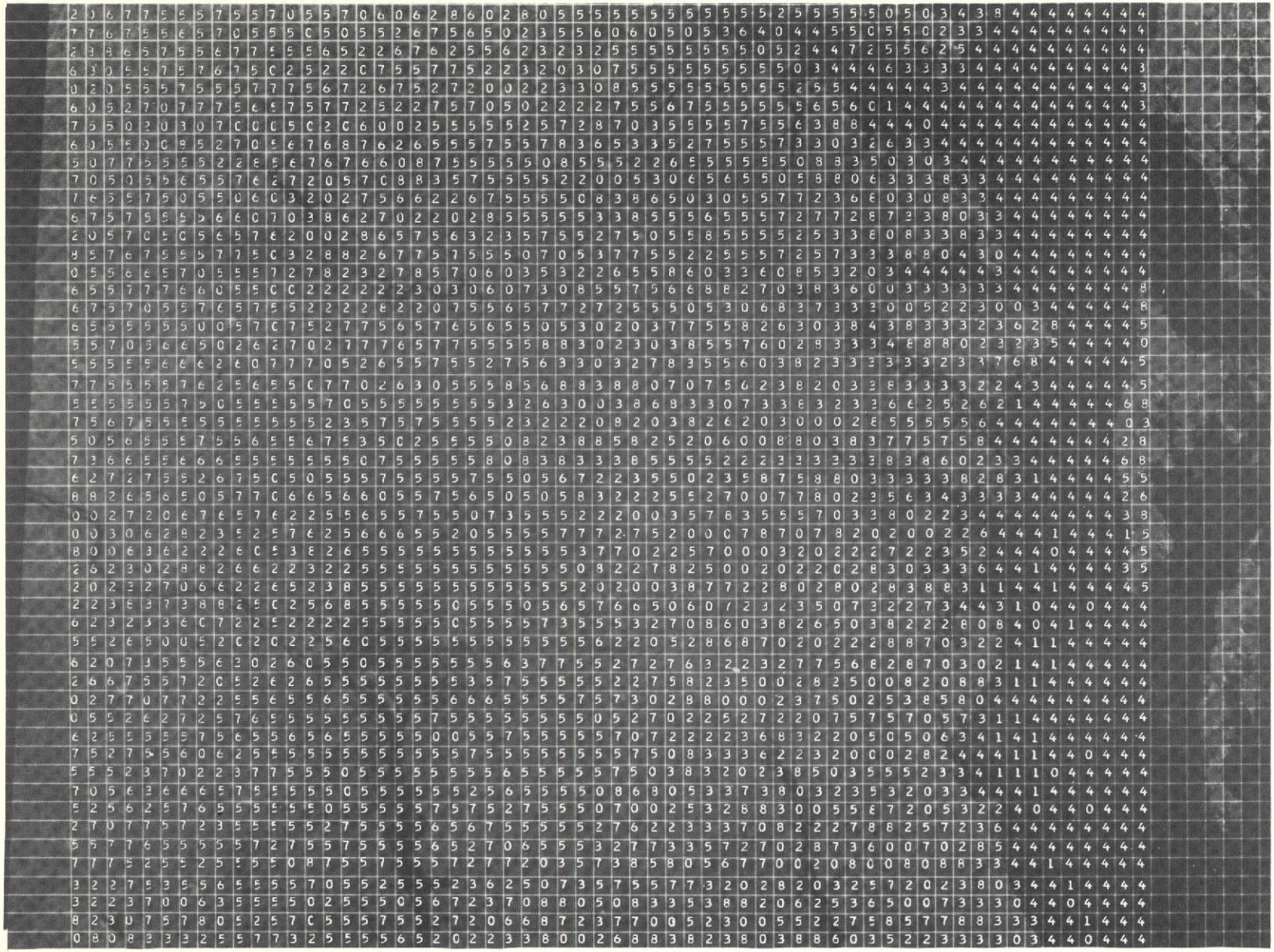

Fig. 5-5 — ERTS-1 image 1080-15192 (Washington, D.C.) with clustering results—operation no. 6 of Table 5-4

The processing operations are summarized in Table 5-5. Operation no. 9 gave the best clustering results. Table 5-6 provides a comparison of the clustering results to the assignments made by photointerpretation. The ERTS-1 image shows the central valley draining into the San Francisco Bay through the Sacramento and San Joaquin Rivers. Between the confluence of the two rivers and Stockton, the central valley appears very wet, possibly due to spring rains. Most of the valley's cultivated area was assigned to class no. 5 including the two rivers, two small lakes and two reservoirs. Water was not recognized as a separate class due to the small number of vectors from this category. It appears that the large farm plots have been assigned to class no. 5. The small farm plots were assigned to class no. 4. This class also includes a large area with vineyards north of Stockton and the urban areas of Stockton and two smaller towns. There were not enough urban vectors to produce a separate urban class. Class 1 represents low barren hills, covered with grass which dries up in the summer. Class 2 represents higher hills covered with brush. Class 3 represents mainly border areas between the hills and the farmed areas. Examination of class 3 assignments shows that class 3 represents large fallow farms.

Figure 5-6 shows the MSS 7 band image of the processed area with the clustering results superimposed as numerical annotations.

5.4 New York City Area

ERTS image 1258-15082 from the New York City area was processed through the clustering algorithm using different threshold values. Table 5-7 summarizes the processing operations on this image. Operation no. 4 produced acceptable clustering results which were photointerpreted. Table 5-8 provides a comparison of the clusters developed to the photointerpreter's assignment of cells to terrain types. The data processed represents New York City, the western part of Long Island, a part of the state of New York north of New York City, the southwestern tip of Connecticut, and northern New Jersey. This area is heavily urbanized and similar to the Washington area. The metropolitan area of New York City and Newark, New Jersey has expanded in all directions with the outlying urban areas being mostly residential. The urban expansion is more pronounced along highways and interrupted by rivers, swamps and the sea. The transition between vegetation (trees) and high building density is a gradual one with the downtown areas having no trees (except in parks) and many residential areas retaining a good density of trees. Farms are small and irregular in shape and interspersed between woods and urban areas. Most of the area northwest of Newark, New Jersey was assigned to cluster 1. This area contains forested hills and small farms. Also, some urban areas with vegetation (mostly residential areas, golf courses and city parks) were also assigned to cluster 1. Two water clusters were developed (clusters 2 and 3) containing exclusively vectors from cells in the Long Island Sound and the Atlantic Ocean. The difference between these two clusters appears to be the quantity of sediment in the sea water. Cluster 4 consists mostly of large farms, some forested areas and a

Table 5-5.
Summary of Processing Operations on Image 1273-18183
Stockton, California

Operation Number	Thresholds*	No. of Zeros	No. of Clusters	Comments
1	NDD = 600 NT = 14 TD2 = 45 TC = -65 TR = 0.85	209	A.† 9 B.‡ 3	Too few final clusters.
2	NDD = 600 NT = 13 TD2 = 45 TC = -65 TR = 0.85	300	A. 10 B. 4	Too few final clusters.
3	NDD = 600 NT = 12 TD2 = 45 TC = -65 TR = 0.85	55	A. 13 B. 5	Abnormal cluster growth.
4	NDD = 600 NT = 13 TD2 = 40 TC = -65 TR = 0.85	208	A. 10 B. 6	Abnormal cluster growth.
5	NDD = 600 NT = 14 TD2 = 40 TC = -65 TR = 0.85	235	A. 9 B. 5	Abnormal cluster growth.
6	NDD = 600 NT = 14 TD2 = 40 TC = -70 TR = 0.85	312	A. 9 B. 5	Fair cluster growth. Two clusters are very large.

* See section 5.1.1 for description of thresholds.

† Initial cluster cores formed before divergence test.

‡ Final cluster cores after divergence test.

Table 5-5.
(Continued)

Operation Number	Thresholds	No. of Zeros	No. of Clusters	Comments
7	NDD = 600 NT = 13 TD2 = 40 TC = -70 TR = 0.85	361	A. 10 B. 6	Fair cluster growth. Two clusters are very large.
8	NDD = 600 NT = 13 TD2 = 40 TC = -75 TR = 0.85	331	A. 10 B. 6	Fair cluster growth. Two excessively large clusters.
9	NDD = 600 NT = 14 TD2 = 40 TC = -75 TR = 0.85	317	A. 9 B. 5	Good clustering results.

Table 5-6. Comparison of Clustering Results

ERTS-1 Image 1273-18183
Stockton, California

Computer	Photointerpreter B	H1	H2	H3	F1	F2	W
0	144	25	16	0	23	109	0
1	0	96	0	0	0	2	0
2	10	0	185	0	0	9	1*
3	0	0	0	75	0	49	0
4	6	← 6 →			815	0	0
5	0	← 32 →			0	1367	86

Detection Rates, %	
All Hills	82
F1	97
F2	89

B = Boundaries

H1 = Intermediate Hills

H2 = High Hills

H3 = Low Hills and Fallow Farms

F1 = Urban, Orchards and Small Farms

F2 = Large Farms and Drainage System

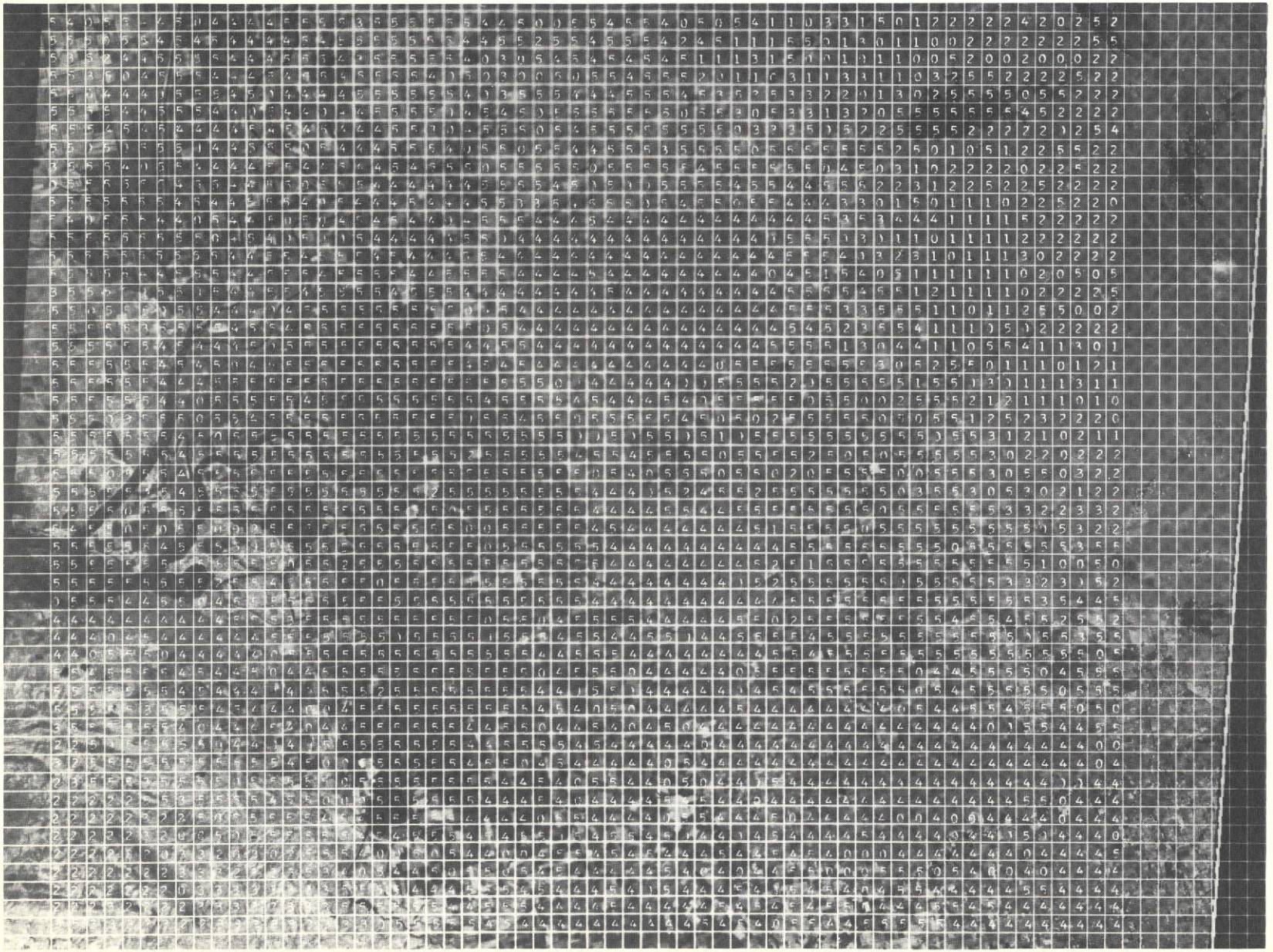

Fig. 5-6 — ERTS-1 image 1273-18183 (Stockton, California) with clustering results

Table 5-7.
Summary of Processing Operations on Image 1258-15082

New York City Area

Operation Number	Thresholds*	No. of Zeros	No. of Clusters	Comments
1	NDD = 600 NT = 14 TD2 = 45 TC = -65 TR = 0.85	212	A† 11 B‡ 5	Poor cluster growth.
2	NDD = 600 NT = 13 TD2 = 45 TC = -65 TR = 0.85	85	A. 15 B. 6	Poor cluster growth.
3	NDD = 600 NT = 13 TD2 = 40 TC = -65 TR = 0.85	313	A. 15 B. 9	Poor cluster growth.
4	NDD = 600 NT = 14 TD2 = 40 TC = -65 TR = 0.85	278	A. 11 B. 6	Good clustering results.

* See Section 5.1.1 for description of thresholds.

† Initial cluster cores formed before divergence test.

‡ Final cluster cores after divergence test.

Table 5-8. Comparison of Clustering Results

ERTS-1 Image 1258-15082
New York City Area

Computer	Photointerpreter B	F1	W1	W2	F2	U1	U2
0	177	13	0	13	36	← 39 →	
1	0	869	0	0	0	← 249 →	
2	0	0	44	0	0	0	0
3	0	0	0	277	0	0	0
4	0	0	0	2	373	← 107 →	
5	0	0	0	6	0	91	5
6	0	0	1	152	0	0	598

B = Boundaries

F1 = Mostly Forest, Some Farms

W1 = Type 1 Water

W2 = Type 2 Water

F2 = Mostly Farms, Some Forest

U1 = Type 1 Urban

U2 = Type 2 Urban

Detection Rates, %	
F1	99
W1	98
W2	62
F2	91
All U	63

few urban residential areas. Cluster 5 consists mainly of urban downtown areas. Cluster 6 contains most of the metropolitan area of New York City and Newark, small rural towns, the Hudson River and some coastal waters in the Hudson River estuary, Long Island and Staten Island.

Considering the complexity of the New York City area, it is obvious that urban areas have been well identified from rural areas and sea water. Figure 5-7 shows the MSS 7 band image with the clustering results superimposed as numerical annotations.

5.5 Hill County, Montana

ERTS image 1376-17452 from Hill County, Montana near the Canadian border was processed through the clustering algorithm twice with slightly different threshold values. The processing operations are summarized in Table 5-9. Operation no. 2 produced good clustering results. Table 5-10 provides a comparison of the clusters produced to the photointerpreter terrain assignments.

The data processed represents mostly an agricultural area bounded on the north by the Fresno Reservoir, east by the Bearpaw Mountains and south by the Missouri River and southeast by the Marias River. The agricultural area consists mainly of rectangular farms of variable size which apparently have been recently harvested. The image was acquired on August 3, 1973. Most of the agricultural area has been assigned to cluster 1. Cluster 3 contains the remaining agricultural fields which are mostly irregular in shape and are located within the lowlands. The lowlands are about 200 feet below the rest of the plain and are located in a wide belt around the western approaches to the Bearpaw Mountains. The plain rises slowly in a northwest direction from the Bearpaw Mountains. Cluster 2 consists mainly of rough terrain between the lowlands and the Bearpaw Mountains. Cluster 2 contains many valleys and streams cutting through the hills surrounding the Bearpaw Mountains. Cluster 4 consists of mountainous terrain in the Bearpaw Mountains which are forested while the surrounding plain appears dry.

There is also the small town of Havre which was assigned to cluster 3, since only a small number of urban vectors exists and a separate urban cluster was not developed. Clouds and their shadows over the Bearpaw Mountains were also not identified as separate clusters due to small numbers of vectors.

Figure 5-8 shows the clustering results superimposed as numerical annotation on the MSS 7 band image.

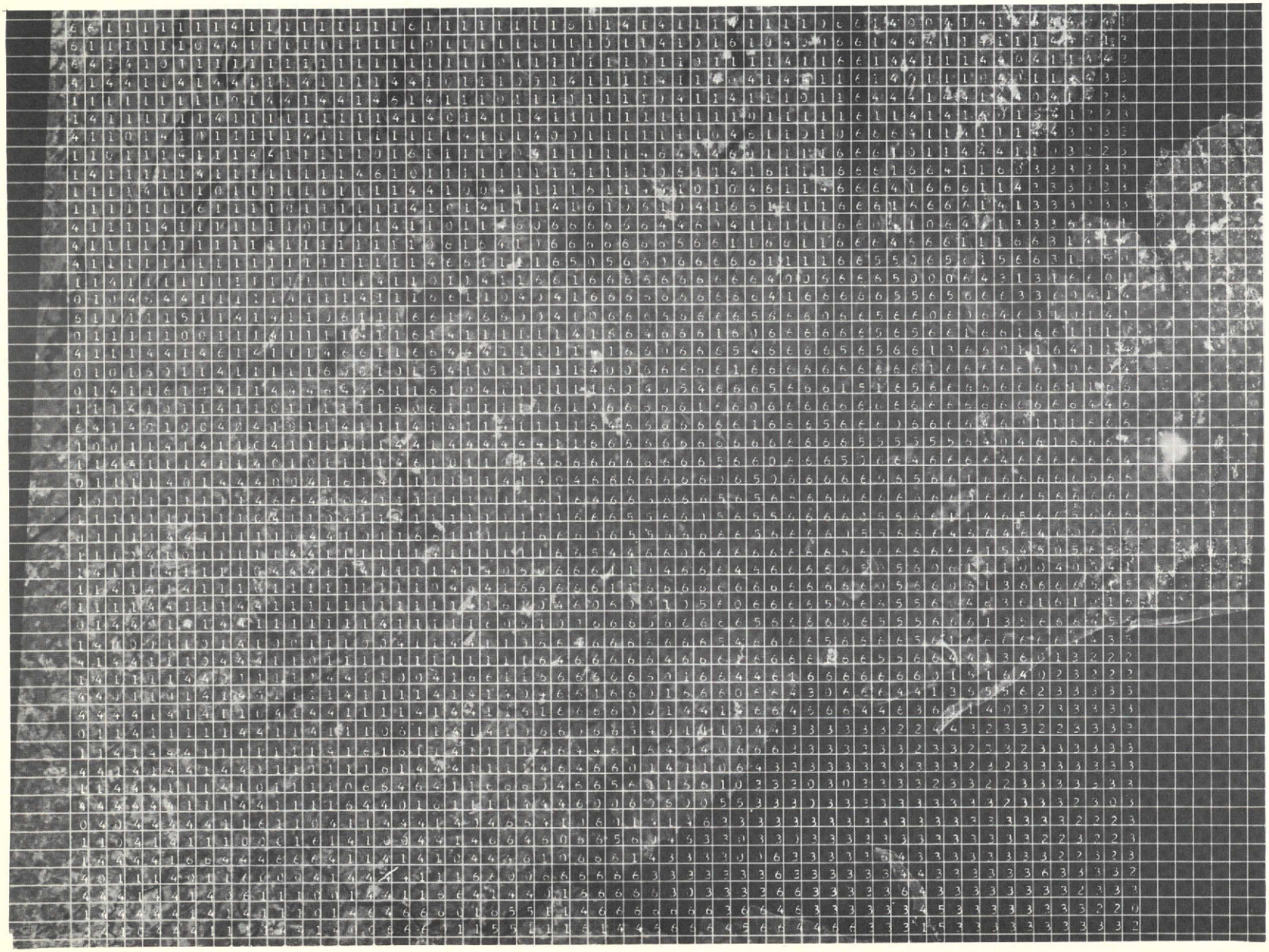

Fig. 5-7 — ERTS-1 image 1258-15082 (New York City Area) with clustering results

Table 5-9.

Summary of Processing Operations on Image 1376-17452
Hill County, Montana

Operation Number	Thresholds*	No. of Zeros	No. of Clusters	Comments
1	NDD = 600 NT = 13 TD2 = 40 TC = -70 TR = 0.85	218	A.† 11 B.‡ 4	Abnormal cluster growth.
2	NDD = 600 NT = 14 TD2 = 40 TC = -80 TR = 0.85	292	A. 9 B. 4	Good clustering results.

* See Section 5.1.1 for description of thresholds.

† Initial cluster cores formed before divergence tests.

‡ Final cluster cores after divergence test.

Table 5-10. Comparison of Clustering Results

ERTS-1 Image 1376-17452
Hill County, Montana

Computer	Photointerpreter B	F	R1	R2	M	C	S	U	W
0	166	78	0	0	39	7	2	0	0
1	0	1534	0	0	0	11	0	0	0
2	0	0	226	0	0	0	0	0	0
3	0	126	0	424	38	15	27	5	0
4	0	1	0	10	289	5	46	1	10

B = Boundaries
F = Farms
R1 = River Banks & Streams
R2 = Flood Plain
M = Hills & Mountains
C = Clouds
S = Cloud Shadows
U = Small City
W = Rivers & Lakes

Detection Rates, %

F	88
R1	100
R2	98
M	79

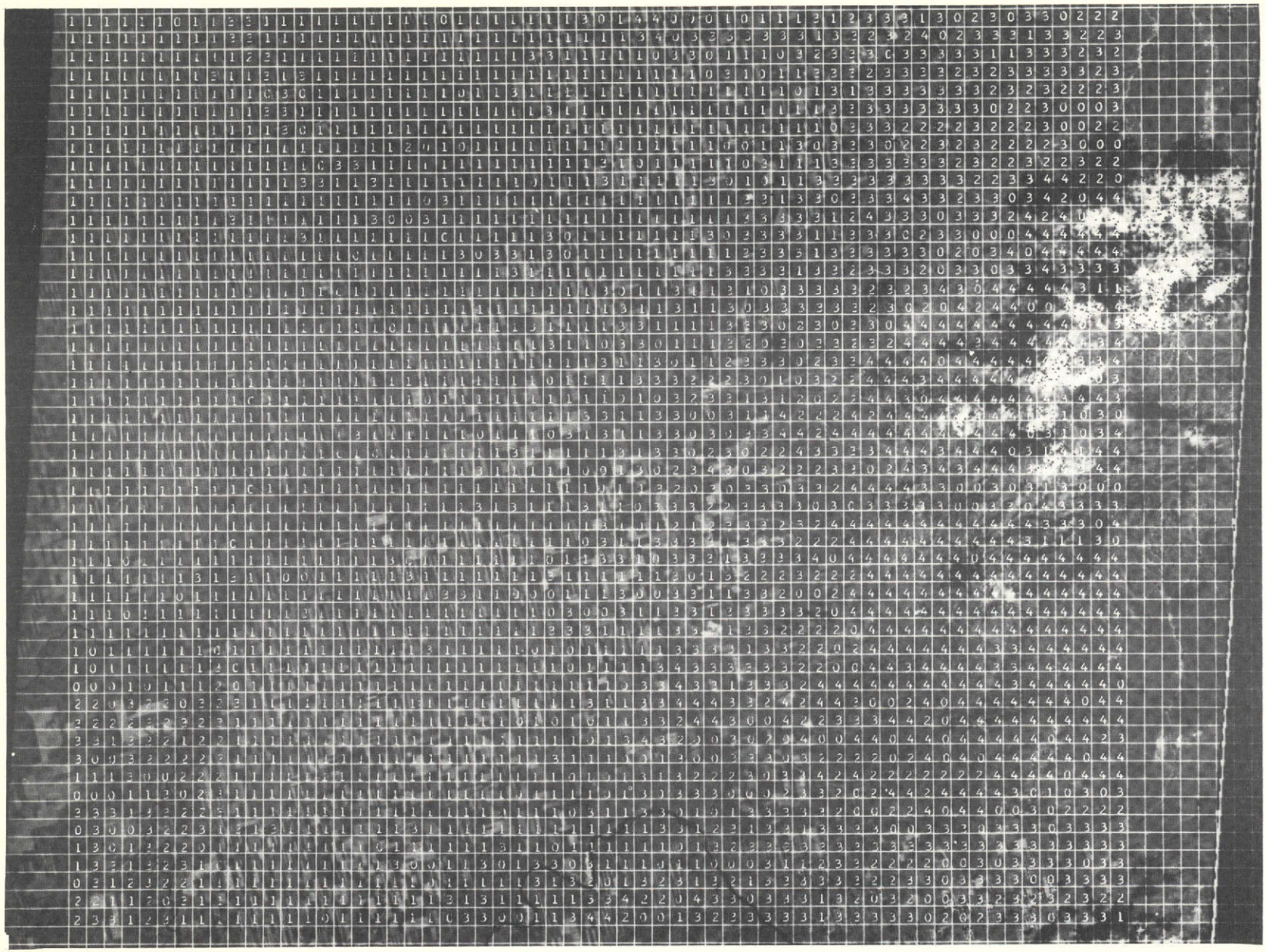

Fig. 5-8 — ERTS-1 image 1376-17452 (Hill County, Montana) with clustering results

6. CONCLUSIONS

During this part of the investigation, it was determined that it is possible to reduce the cell size to less than 32 x 32 pixels. One need only be careful with the feature amplitude normalizations. Also, the Fourier transforms of cells should be interpolated to reduce the quantization noise in the spatial features.

As the cell size is reduced, it was determined that the recognition of terrain becomes gradually less accurate. For the smaller cell sizes such as 9 x 9 pixels or 13 x 13 pixels, fewer clusters are produced and they represent specific terrain types less accurately. Examination of feature statistics and cluster divergences disclosed that the clusters become more diffuse and less statistically separable as the cell size is reduced.

A major development of this part of the investigation is the demonstration that 17 x 17 pixel cells can be used effectively with the clustering algorithm to recognize major terrain types and terrain subclasses with high accuracy. The generation of subclasses can be achieved with 17 x 17 pixel cells without processing the data at several cell sizes. The subclass formation depends on the geographic location represented by the data and the threshold values employed in the clustering algorithm.

The ERTS images processed through the clustering algorithm with 17 x 17 pixel cells provided a thorough evaluation of the clustering algorithm operation. An understanding of the effects of the algorithm's thresholds on the formation and growth of clusters was developed. A substantial number of images has been processed through the clustering algorithm with 32 x 32 pixel cells in the first part of the investigation and with 17 x 17 pixel cells in the second part of the investigation. Comparing the clustering results between these two cell sizes, it appears that the 32 x 32 pixel cells provide slightly higher recognition accuracies on the major terrain types with an average detection rate of 89%. The average detection rate of the terrain types for the 17 x 17 pixel cells is 82%. There are certain definite advantages in using the smaller cells. For a given geographic area, there will be 3.5 times more 17 x 17 pixel cells than 32 x 32 pixel cells. When 17 x 17 pixel cells are employed, boundary cells containing more than one terrain class constitute a smaller percentage of the total number of cells and boundaries between terrain classes can be determined more accurately. In addition, the smaller cell size favors the formation of urban clusters. If 32 x 32 pixel cells are used, a single city should have an area larger than about 100 square kilometers in order for an urban cluster to emerge, assuming that 16 vectors are required for the cluster. If 17 x 17 pixel cells are used, a single city should have an area larger than 29 square kilometers so that an urban cluster with at least 16 vectors can be formed. Similar arguments can also be made for other terrain classes. The main

conclusion is that for a specific geographic area the 17 x 17 pixel cell favors the creation of more terrain clusters because it provides 3.5 times more vectors than the 32 x 32 pixel cell. A compensating effect is, of course, the increased diffuseness of the clusters as the cell size is reduced, which diffuseness becomes evident in the reduced detection rates for the terrain clusters. Therefore, one must select the cell size so as to balance the requirements for more terrain resolution in terms of the number of clusters formed and the geographic location accuracy offered by the smaller cell against the terrain recognition accuracy represented by the detection and false alarm rates. It appears that the 17 x 17 pixel cell is the best compromise as a nominal cell size for most geographic regions. It is conceivable though that one may desire to increase or decrease the cell size depending on the specific geographic region and his terrain accuracy requirements.

7. RECOMMENDATIONS

It is recommended that the software system and the pattern recognition techniques developed under this investigation be applied on many problems of national importance for which remote sensing of the earth by the ERTS-1 satellite can provide very valuable information. The following applications are suggested as being potentially of high economic value:

a. Monitoring of agricultural crops and forest resources to detect crop stresses and estimate crop yield.

b. Uniform land-use mapping for the entire country.

c. Monitoring of snow fields to predict flooding and estimate water resources.

d. Detection of water pollution.

The utility of the interpretation techniques and the software system developed is appreciated when one examines Figures 5-1 through 5-8, which show the clustering results superposed on the MSS 5 band images. For example, in the New York City area (Figure 5-7) the urban areas have been identified by clusters 5 and 6, and have been correctly separated from the rural areas (clusters 1 and 4) and the Atlantic Ocean (clusters 2 and 3). It appears that the clustering algorithm has extracted most of the terrain information available in this ERTS-1 image. The output of the clustering algorithm is a simple land use map which was produced very rapidly by machine processing and with a minimum of human supervision.

Two and one-half hours on an IBM 370 time shared computer are required to preprocess and compute 3,060 feature vectors representing an area of 43 x 50 square nautical miles. One half of an hour on the same computer is then needed to process these vectors through the clustering algorithm. In comparison, it is estimated that a photointerpreter may require one to two weeks of tedious work to produce a similar land use map. The software developed could be made more efficient in terms of computer time if one desired to process a lot of ERTS-1 data and was particularly concerned about the cost of computer time. It is estimated that the processing time could be reduced to substantially less than one hour by making the software more efficient. Thus, machine processing appears to be cost effective in relation to manual photointerpretation. In addition, it is the only practical method of processing the massive volume of data produced by the earth resources satellites. Furthermore, machine processing is expected to become more cost effective in the near future as advances in microelectronics make possible more powerful, low-cost computers.

Experience with the processing software developed, and in particular the clustering algorithm, indicates that it is desirable for a human operator to control the processing operations. In our processing system, this is done by selecting a few thresholds and the software is stuctured so that the operator can effectively observe the formation and growth of the clusters. This approach which has worked very well points to an interactive system using small computers with an operator, who observes the processing operations, and controls them in real-time. In such a system, the hardware executes the tedious classification tasks while the operator guides the machine to accomplish the required classification functions.

It is recommended that the software classification system developed from this investigation be utilized to process more ERTS data for specific resource management goals, such as land use, urban planning, management of forests, etc.

9. REFERENCES

1. Gramenopoulos, N. Automated Thematic Mapping and Change Detection of ERTS-1 Images, Final Report, July 1974, NASA-CR-139221, E74-10688.

2. Gramenopoulos, N. and Alpaugh, H. Automated Thematic Mapping and Change Detection of ERTS-1 Images, Photointerpretation Results of ERTS-1 Images from the Brownsville, Texas Area, December 1972, NASA-CR-129930, E73-10006.

3. Goodman, Joseph W. Introduction to Fourier Optics, McGraw-Hill Book Co., Inc., New York (1968), p. 86.

4. Gramenopoulos, N. and Corbett, F. J. Automatic Thematic Mapping and Change Detection of ERTS-1 Image, Diffraction Pattern Analysis of ERTS-1 Images, March 1973, NASA-CR-131054, E73-10385.

5. Gramenopoulos, N. Terrain Type Recognition Using ERTS-1 MSS Images, NASA SP-327, Symposium on Significant Results Obtained from the Earth Resources Technology Satellite-1, March 5-7, 1973.

6. Wacker, A. G. and Landgrebe, 1970, Boundaries in Multispectral Imagery by Clustering, Proceedings of 9th IEEE Symposium on Adaptive Processes, XI, pp. 4.1 - 4.8.

7. Swain, P. H. Pattern Recognition: A Basis for Remote Sensing Data Analysis, LARS, Purdue University, Lafayette, Indiana, NASA-CR-130757, LARS-111572, N73-17184.

8. Marill, T. and Green, D. Statistical Recognition Functions and the Design of Pattern Recognizers, IRE Transaction on Electronic Computers, December 1960, p. 472.

9. Poulton, E. C., Schrumpf, B. J., and Johnson, J. R. Ecological Resource Analysis from High-Flight Photography for Land Use Planning, Applied Remote Sensing of Earth Resources in Arizona, Proceedings 2nd ARETS Symposium, University of Arizona, November 2-4, 1971.

10. Marill, T. and Green, D. On the Effectiveness of Receptors in Recognition Systems, IEEE Transactions on Information Theory, January 1963, p. 11.

9. REFERENCES
(Continued)

11. Anderson, J. R., Hardy, E. E. and Roach, J. T. A Land-Use Classification System for Use with Remote-Sensor Data, Geological Survey Circular 671, 1972, Washington.

12. Gramenopoulos, N. Automated Thematic Mapping and Change Detection of ERTS-A Images, December 1972, NASA-CR-129251.

13. Gramenopoulos, N. Automated Thematic Mapping and Change Detection of ERTS-A Images, August 1973, NASA-CR-136556, E74-10236.

14. Corbett, F. J. Terrain Recognition in ERTS-1 Imagery by Diffraction Pattern Analysis, Proceedings of the American Society of Photogrammetry, Fall Conference, Lake Buena Vista, Florida, October 2-5, 1973, Library of Congress Catalog Number 73-86064.

15. Gramenopoulos, N. Automated Thematic Mapping and Change Detection of ERTS-1 Images, Proceedings of the American Society of Photogrammetry, Symposium on Management and Utilization of Remote Sensing Data, Sioux Falls, South Dakota, October 29 - November 1, 1973, p. 432.

16. Gramenopoulos, N. Automated Thematic Mapping and Change Detection of ERTS-1 Images, Proceedings of the Annual ARETS Conference, November 4, 1973, Tucson, Arizona.

17. Gramenopoulos, N. Automated Thematic Mapping and Change Detection of ERTS-1 Images, Third Symposium of ERTS-1 Principal Investigators, December 10-13, 1973, Washington, D. C.